Phenotypic characterization of a *Mycobacterium smegmatis* strain lacking MSMEG_0858

Vuyani Branti (920099)

A dissertation submitted to the Faculty of Health Science, University of the Witwatersrand, Johannesburg, in fulfilment of the requirements for the degree of Master of Science in Medicine.

June 2021

Abstract

The genus Mycobacterium represents a complex family containing a number of clinically significant pathogens such as *Mycobacterium tuberculosis* (*Mtb*), *Mycobacterium ulcerans, and Mycobacterium leprae*. Tuberculosis remains a global health issue, claiming approximately two million lives annually, with much of this burden occurring in developing countries such as India and South Africa. Due to the emergence of drug-resistance, there is an urgent need to identify drugs with novel modes of action or different drug targets. In this regard, mycobacterial proteins that are essential for various cellular processes may serve as a starting point for the identification of potential targets. This study focuses on the protein product of MSMEG_0858, Cdc48, which is a member of the AAA+ protein family involved with protein homeostasis via direct interaction with the 20S proteasome. A previous study suggested that Cdc48 interacted with an essential peptidoglycan associated enzyme (MSMEG_6113, DacB). This study aimed to explore this further. A *Mycobacterium smegmatis* (*Msm*) strain lacking MSMEG_0858 was phenotypically characterized using several assays but prior to this, the strain was genotypically confirmed using PCR, Southern hybridization and mRNA transcript analysis. The mutant strain was shown to be dispensable for growth in 7H9 (nutrient rich) media, but when cultured in carbon-limited media lacking glycerol, growth rate was reduced, an observation that was reversed following genetic complementation. The Δ*cdc48* strain was more permeable to EtBr uptake but despite this, no differences in sensitivity to several antibiotics (including amoxicillin, vancomycin and D-cycloserine), cell damaging agents (lysozyme and formaldehyde), heat-shock or exposure to detergents (SDS), were observed. Collectively, our observations suggest a non-essential role for Cdc48 under nutrient-rich conditions. Under carbon-limiting conditions, the protein may play a more central role but more work is required to describe the physiological mechanism and to target this protein for drug development against *Mtb*.

Declaration

I, **Vuyani Branti**, declare that this dissertation is my own work. It is being submitted for the degree of Master of Science in Medicine at the University of the Witwatersrand, Johannesburg. It has not been submitted before for any degree or examination at this or any other university.

Vuyani Branti

Date: _25__ of ___June____, 2021

Place: Johannesburg, South Africa

Dedication

This work is devoted to my family and friends.

Acknowledgements

I wish to show my appreciation to my supervisor Dr. Christopher Ealand who supported, encouraged and guided me during the period of this study as well as Prof. Bavesh Kana who gave me this amazing opportunity to do this project on the topic “Phenotypic characterization of a *Mycobacterium smegmatis* strain lacking MSMEG_0858” in his lab.

I would also like to extend my especial thanks to my colleagues who assisted me a lot in completing this project over a limited period.

Table of Contents

List of figures

List of tables

Nomenclature and Abbreviations

µ	Micro
AAA	ATPases associated with various cellular activities
AG	Arabinogalactan
ATP	Adenosine triphosphate
attB	tRNAGly attachment site
bp	base pairs
CFUs	colony forming units
CTAB	Cetyltrimethylammonium bromide
D-ala	D-alanine
D-gln	D-glutamine
D,D-CPases	D,D-carboxypeptidases
DNA	Deoxyribonucleic acid
dNTPs	Deoxynucleotide triphosphate
EtBr	Ethidium bromide
g	grams
Hyg	Hygromycin
L-ala	L-alanine
LMM	Low molecular mass
LTBI	Latent TB infection

m	milli
M	Molar
MA	Mycolic acid
mDAP	meso-diaminopimelic acid
MDR-TB	Multi-drug resistant TB
MIC	Minimum inhibitory concentration
Msm	*Mycobacterium smegmatis*
Mtb	*Mycobacterium tuberculosis*
min	minutes
n	nano
NaCl	Sodium chloride
NAG	*N*-acetylglucoseamine
NAM	*N*-acetylmuramic acid
OD_{600nm}	Optical density at 600 nanometer wavelength
PBPs	Penicillin binding proteins
PBS	Phosphate buffered saline
PCR	Polymerase chain reaction
PG	Peptidoglycan
rpm	Revolutions per minute
sec	seconds
SDS	Sodium dodecyl sulphate
TB	Tuberculosis
UDP	Uridine diphosphate
WHO	World Health Organization
XDR-TB	Extensively-drug resistant TB

1. Introduction

1.1 Tuberculosis

Tuberculosis (TB), caused by the bacterial pathogen *Mycobacterium tuberculosis* (*Mtb*), is a disease that primarily affects the lungs. Despite being curable, TB still poses a major threat to global health (WHO, 2013). In 2017, it was reported 10 million people were infected with TB and 1.6 million people died from the disease (MacNeil et al., 2019). TB is transmitted from person to person through the air, i.e. when an infected individual coughs, sneezes or spits, *Mtb* is propelled into the air and a susceptible individual only needs to breath in a few of these aerosolized particles to get infected . Symptoms for TB include night sweats, coughing, weight loss and fever. These symptoms may also be mild resulting in delayed treatment and subsequent increased transmission events (Agyeman and Ofori-Asenso, 2017). It has been estimated that about one-third of world's population harbours a latent TB infection (LTBI) (Boshoff and Barry, 2005). This form of the disease is associated with no clinical symptoms and patients are not infectious but there is a risk of progressing to an active infection (Andrews et al., 2012). Individuals who have a latent infection together with compromised immune systems, including people living with HIV, diabetes, malnutrition and those using tobacco, have a higher risk of progressing to active TB (Lönnroth et al., 2010). Active, drug-sensitive TB is treated with combination of four antimicrobials over a period of six to nine months (Hoagland et al., 2016). However, the emergence of drug resistant TB (i.e. multi-drug resistant (MDR) or extensively drug-resistant (XDR)-TB) has become a major public health crisis (Gandhi et al., 2010). Infections with drug resistant strains will not respond to first-line TB drugs (Iseman, 1993) and may occur because of poor patient compliance, inferior quality drugs and inappropriate prescription by health care providers. Drug-resistant TB is curable using second-line antibiotics that require extensive chemotherapy of up to two years of treatment, but these are expensive and

are often associated with severe side-effects (Falzon et al., 2017). **Figure 1.1** shows a list of high burden countries for TB, TB/HIV and MDR-TB as reported by WHO for the period 2016–2020. There is therefore an urgent need to identify novel drugs to circumvent these limitations. Before this is achievable, a comprehensive understanding related to transmission patterns and bacterial pathogenesis of TB is required (Organization).

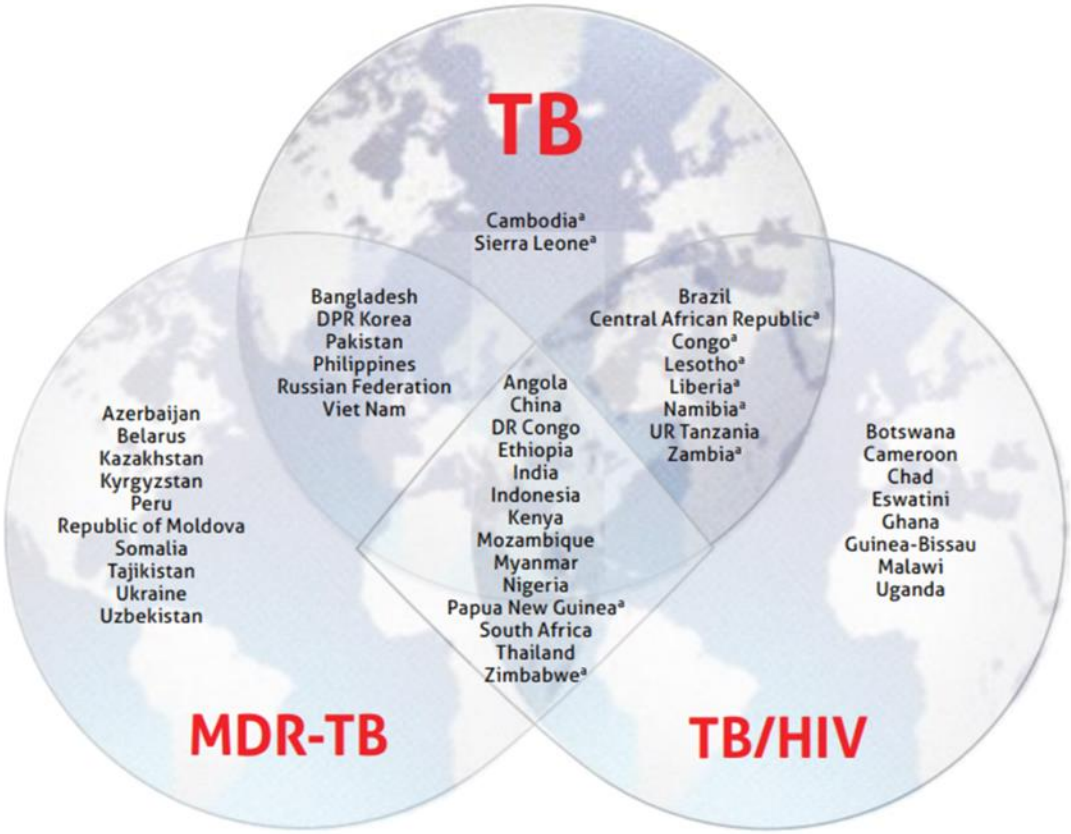

Figure 1.1. List of thirty countries with the highest TB burdens. This list was based on TB burden severity (i.e. incident cases per 100 00 population per year), as opposed to the top 20 countries, which are included based on total number of incident cases per year.

1.2 *M. tuberculosis* pathogenesis and tuberculosis infection

Mtb is carried in airborne particles – called droplet nuclei or aerosolized particles – which range from 1-5 microns in diameter (Nardell, 2016). When a person with active pulmonary TB coughs, sneezes or spits, droplet nuclei are generated and suspended in the air which can remain there for several minutes to hours (Lokhande and Pawar, 2019). Inhalation of droplet nuclei, containing *Mtb* may result in TB infection. The droplet nuclei reach the alveoli of lungs where the pathogen encounters the alveolar macrophages and dendritic cells. Alveolar macrophages and dendritic cells present mannose and complement receptors that recognise the bacilli leading to the internalisation of the bacilli by phagocytic antigen-presenting cells in the lung including alveolar macrophages and dendritic cells. Phagocytosis triggers the host immune response in an attempt to inhibit further growth of the tubercle bacilli. The activated T lymphocytes, macrophages, and other immune cells form granuloma which are required for control of the disease and represent a critical immunological feature. Granuloma are composed of epithelial macrophages, neutrophils, and other immune cells surrounded by fibroblasts. If granulomas remain intact, it is possible for a latent TB infection to develop (Agyeman and Ofori-Asenso, 2017, Ramakrishnan, 2012, Marakalala et al., 2016). *Mtb* is well adapted to evade the host immune system. When the foreign organism is engulfed by macrophages, it is stored in the phagosome, which then matures following fusion with lysosome, exposing the contents to acidic pH, oxygen radicals and degradative enzymes such as lysosome leading to destruction. Phagosome maturation is dependent on calcium ion signalling and *Mtb* has mechanisms to prevent phagosome-lysosome fusion, likely by inhibiting the calcium ion signalling (de Martino et al., 2019). The *Mtb* cell wall is characterized by abundance of mycolic acid enclosed by a capsule layer consisting of lipids and polysaccharides. These molecules may interact with receptors of the host cells such as toll-like receptors, leading to the production of pro-inflammatory cytokines such as interleukin (IL)-1, tumor necrosis factor (TNF)-α, IL-12, and chemokines. Lipoprotein of *Mtb* regulate antigen

presenting cell function and TLR2 is activated by innate immunity. Studies have shown that a continuous signalling via TLR2 by lipoproteins of *Mtb* prevents the expression of major histocompatibility complex (MHC)-II and processing of antigens by macrophages (Noss et al., 2000). Therefore infected macrophages displaying low number of antigen-presenting cell function may be unable to present *Mtb* antigens to CD4+ T cells leading in insufficient activation of effector T cells resulting to an evasion of immune surveillance and creation of environment where Mtb survives and persists (Harding and Boom, 2010).

1.3 Diagnosis and treatment of tuberculosis

Several diagnostic tools are used to identify *Mtb* infections. Active TB is differentiated from latent TB via the presence or absence of clinical symptoms. . The tuberculin skin test (TST) is based on injecting the arm with a tuberculin purified protein derivative (PPD). An inflammatory response results in the formation of a bump (within 72 hours) due to current or prior TB infection. Normally the test results are read after 48 to 72 hours (Suleiman, 2017). The interferon gamma release assay (IGRA) measures T-cell release of IFN-Ɣ following stimulation by antigens specific to the *Mtb* complex (Barry et al., 2009, Suleiman, 2017). IGRAs are more sensitive and specific than the TST. Individuals who were previously BCG vaccinated may yield a false positive response while those with compromised immune systems may present false negatives. Neither test can accurately differentiate between LTBI and active TB; reactivation or re-infection; or resolve the various stages within the spectrum of *Mtb* infection (Mahomed et al., 2011). For the reason outlined above, it is necessary to confirm the results of these tests using chest x-rays, smear microscopy for the presence of acid-fast bacilli and culture-based methods (such as MGIT or MPN assays) (Chengalroyen et al., 2016). Since fluorescence microscopy techniques (using auramine-O or Zeihl-Neelson staining) are relatively cheap and fast to perform, these tests are frequently used to detect active TB, especially in low-resource settings (Hanscheid et al., 2007).

However, smear microscopy is less sensitive than culture-based methods that select for mycobacterial species. The most specific diagnostic tools employ the amplification and detection of nucleic acids (including the GeneXpert and HAIN line probe assays (LPAs)) specific for *Mtb*. In addition, analysis of nucleic acid sequences may inform of drug susceptibility patterns to inform appropriate selection of drug regimens (Suleiman, 2017).

Despite of all this, improved diagnostic tools are required to detect TB as variation in The clinical presentation makes accurate diagnosis and treatment a challenge (Aricha et al., 2019). The current globally recommended chemotherapy (WHO et al.,2017) by WHO for the treatment of drug-sensitive TB (DS-TB) involves an intensive, two-month phase of four first line drugs (including rifampicin (RIF), isoniazid (INH), pyrazinamide (PYZ) and ethambutol (EMB)) followed by a continuation phase of RIF and INH for the next 4 months. First-line TB drugs are very effective in clearing the pathogen provided the patient carefully adheres to the treatment plan. Second-line drug regimens recommended by WHO for the treatment of MDR-TB include several fluoroquinolones (e.g. ofloxacin, ciprofloxacin, moxifloxacin or levofloxacin), aminoglycosides (e.g. kanamycin or amikacin), capreomycin, cycloserine, para-amino salicylic acid and thioamides (e.g. ethionamide, prothionamide). MDR-TB occurs as a result of resistance to the first-line drugs (WHO, 2017, Bolscher et al., 2007). XDR-TB is a relatively rare type of drug-resistant TB but is on the increase. XDR-TB is classified as resistance to INH and RIF, plus any fluoroquinolone and at least one of three injectable second-line drugs (i.e. amikacin, kanamycin, or capreomycin) (Coker, 2004). Because XDR-TB is resistant to first-line TB drugs and second-line drugs, patients are left with treatment options that are expensive, less effective and with severe side-effects. Emergence of drug resistance may be attributed to genetic mutations, drug compound extrusion by efflux pumps, and the production of enzymes that may degrade antibiotics (e.g. the inactivation of β-lactam antibiotics by β-lactamases) (Singh et al., 2020). The majority of anti-TB drug

compounds target the biosynthesis of mycobacterial cell wall components which are essential for bacterial survival and viability (Abrahams and Besra, 2016).

1.4 The mycobacterial cell wall

The mycobacterial cell wall (CW) is a multi-layered structure that provides a highly selective barrier that is important for cell growth, resistance to antibiotics and virulence making it an attractive target for TB drugs (Bansal-Mutalik and Nikaido, 2014). The core structure is composed of three components, i.e. mycolic acids (MAs), arabinogalactan (AG) and peptidoglycan (PG). This core is surrounded by a capsule comprised of lipids and proteins (**Figure 1.2**) (Hett and Rubin, 2008).

MAs consist of α-alkyl and long β-hydroxyl-fatty acids with 60 to 90 carbons per chain. MA are linked to the AG layer by an ester covalent bond and exist as tetramycolyl-pentaarabinofuranosyl cluster on AG. AG is polysaccharide made of arabinan and galactan. Galactose linkages alternate 1 to 5, 1 to 6. Arabinan is bound to the 5 position of galactan in 1 to 5 linkages. AG is covalently bound by a phosphoryl–*N*-acetylglucosaminosyl–rhamnosyl linkage to the PG layer (Abrahams and Besra, 2016, Besra and Brennan, 1997). PG is a versatile material rigid in maintaining shape and protecting the bacteria against osmotic turgor pressure and while allowing the bacteria to grow and expand. PG is comprised of long strands of alternating *N*-acetyl muramic acid (NAM) and *N*-acetyl glucosamine (NAG) connected via β-1,4 glycosidic bonds. The glycan strands are cross-linked by peptide stems attached to the NAM residues (Squeglia et al., 2018, Scheffers and Pinho, 2005). The penta-peptides side-chains consists of L-alanyl-D-iso-glutaminyl-mesodiaminopimelic acid (mDAP) and two terminal D-alanine residues. The mDAP from one peptide side-chain is linked to the 4th D-alanine residue on an adjacent stem peptide to form a 4-3 cross-link. Alternatively, PG can be remodelled to form a cross-link between two mDAP peptides to generate 3-3 cross-links (Sibinelli-Sousa et al., 2021). Biosynthesis and remodelling – mediated

by the actions of penicillin binding proteins (PBPs) – of PG has been shown to play an important role in adaptation to environmental stresses, including susceptibility to CW-targeting antibiotics (Baranowski et al., 2018). A previous study in the lab (Mashilo, 2018) identified an interesting protein-protein interaction between a low molecular weight (LMW) PBP, DacB and a protein associated with general protein homeostasis (i.e. MSMEG_0858 or Cdc48). A literature review failed to clarify this interaction in mycobacteria or other bacterial species. As a result, the effect of Cdc48 on overall mycobacterial physiology in addition to PG metabolism became the focus of this study.

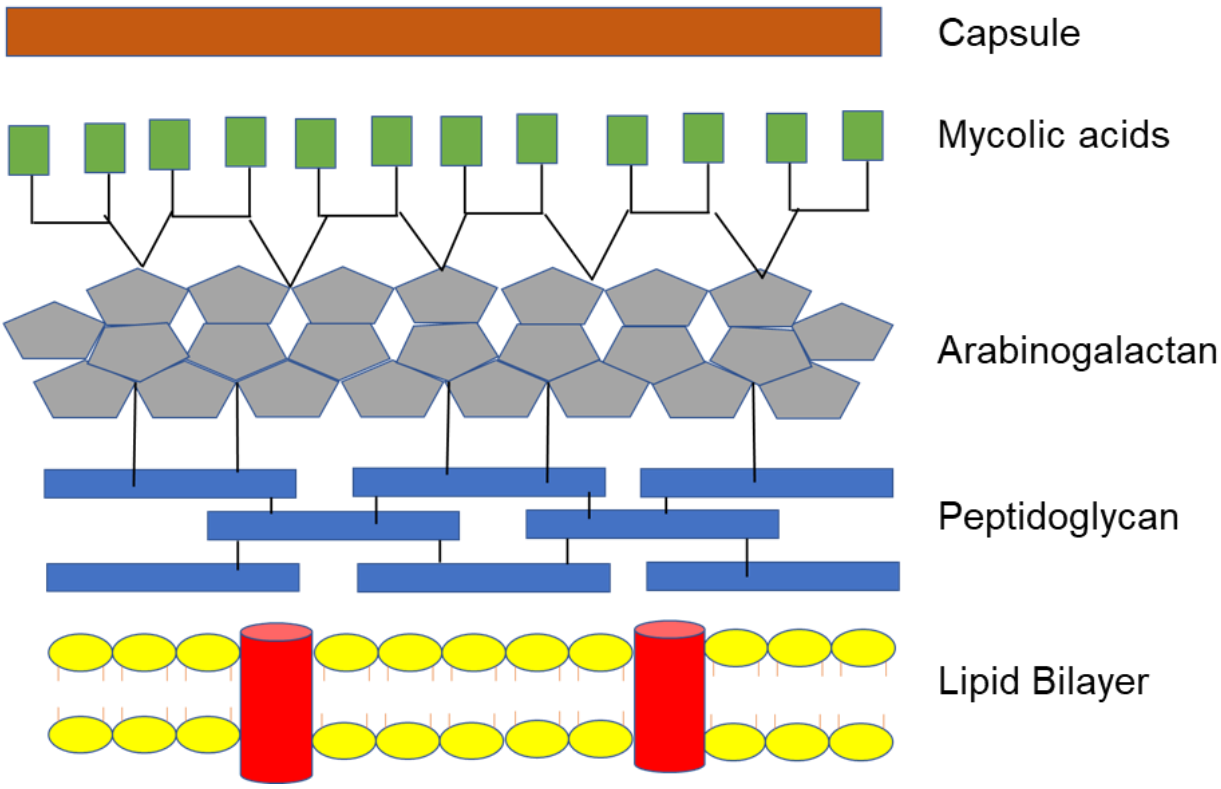

Figure 1.2. A model representing the composition of a typical mycobacterial cell wall. The mycobacterial cell wall consists of an outer most, capsule-like layer made up of proteins and lipids (orange rectangle), mycolic acids (green squares), arabinogalactan (grey pentagons) and peptidoglycan (blue rectangles) cross-linked via peptide side-chains. All of these components surround the lipid bilayer (yellow circles).

1.5 Protein quality control in prokaryotic cells

The regulation of intracellular proteins is an essential process for many aspects cellular biology. Protein quality control plays a vital role in eliminating toxic protein compounds such as aborted translational products, misfolded and damaged proteins. It may also influence metabolic pathway functions, signal transduction and cell division processes via the degradation of key enzymes and transcription factors. Degradation and recycling of proteins may also ensure the supply of amino acids and intermediate metabolites during 'normal' growth and division or under nutrient-limiting conditions (Buchberger, 2013). If a protein becomes damaged or is no longer needed, cells must dispose of it. The proteasome is a barrel-shaped molecular machine that breaks down unwanted proteins. The proteasome binds to other molecules called regulators, which select the proteins to be dismantled. The proteasomes of mycobacteria – a group that includes the bacteria that cause tuberculosis – help them to survive hostile or rapidly changing environments. Mycobacteria possess a molecule called MSMEG_0858 (Cdc48) whose structure is like a regulator that is found in many non-bacterial cells (Ziemski *et al*., 2018).

1.5.1 The role of Cdc48 protein in bacterial protein homeostasis

Cdc48 is classified as an AAA+ ATPase protein. This protein family is represented in all taxa and commonly possess proteolytic activities (Alhuwaider and Dougan, 2017). In eukaryotic organisms, Cdc48 also referred to p97 protein is associated with protein homeostasis – it is a widely conserved 78 kDa protein and plays an important role in the ubiquitin (Ub) proteasome system and it may be responsible for cell survival under adverse environmental conditions. Its

activity is not only limited to direct interaction with ubiquitinanted proteins to regulate turnover, but it also serves as hub for docking of various co-factors (Haines, 2010, Torrecilla et al., 2017). This gives the sight to the function of the mycobacterial homologue (for *Msm*), MSMEG_0858, which is similarly composed of an N-terminal and two AAA+ domains (**Figure 1.3**). Although a second AAA+ domain (D2) in MSMEG_0858 shows a consensus sequence in both motifs, essential residues in the first AAA+ domain have been replaced in both motifs: Thr in walker A has replaced with Val and in walker B Asp has been replaced with Ala (Unciuleac et al., 2016). Despite these changes, both domains of MSMEG_0858 possess ATPase activity indicating both domains can bind and hydrolyse ATP. This protein is a magnesium dependent ATPase. In a recent study it was found crystal structure of both domains of MSMEG_0858 to have high similarities with equivalent domains of p97 in mammals with a root mean square of deviation of 1.5 and 2.4 A, respectively. In the mammalian p97 homologue, the N-terminal serves as platform for docking cofactors and hence it has diverse activities (Förster et al., 2014, Meyer and Weihl, 2014).

This suggests MSMEG_0858 could play wide range functions in mycobacteria. AAA+ proteases have been associated with various biological functions in the cell, including DNA replication, recombination, transcription, remodelling of macromolecules complexes, protein quality, proteolysis, proteins and nucleic acid translocation and membrane fusion (Neuwald et al., 1999).

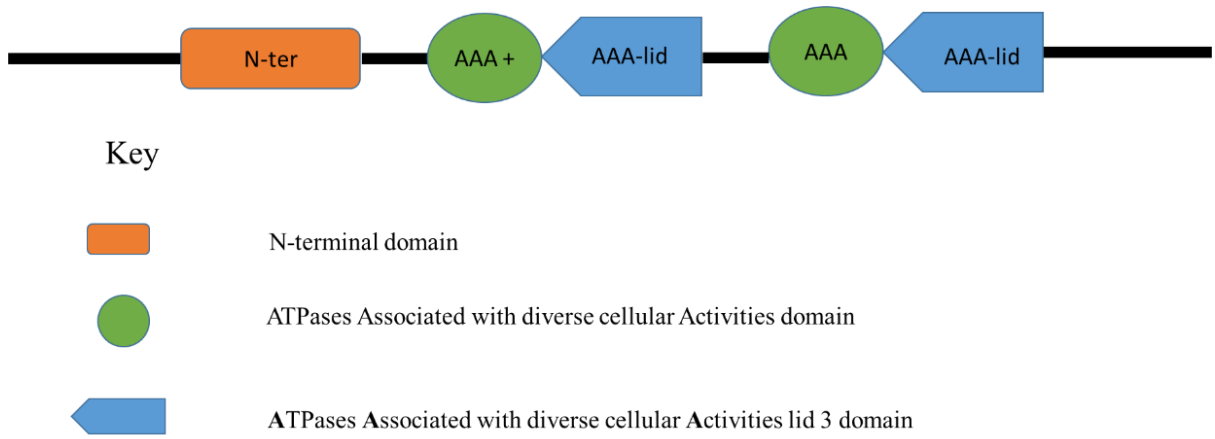

Figure 1.3. Structural feature of the MSMEG_0858 protein. The functional domains are represented by different colours. Shown in blue is the N-terminal domain and in red are the two AAA domains (D1 and D2). The conserved AAA domains each contain the signature nucleotide binding and hydrolysis motifs. Both D1 and D2 domains are capable of ATP hydrolysis however, under physiological conditions D1 shows weak ATPase activity.

Several mycobacterial AAA+ proteases have previously been biochemically characterized, including the essential casein lytic proteins (Clp) proteases ClpC1 and ClpX; the proteasome ATPase Rv2115c; FtsH and zinc metalloproteases (Ziemski et al., 2018, Unciuleac et al., 2016).

FtsH is an AAA+ protease involved in proteolytic degradation of specific cytosolic proteins. FtsH plays a role in the degradation of heat shock transcription factor σ32 and it monitors the levels of phage λCII protein during infection. Cdc48 and FtsH share a common protein motif, both proteins belong to the same family AAA+ proteins and it is plausible that Cdc48 may function in an analogous manner or influence the levels of FtsZ either directly or indirectly by degrading proteins required to stabilize FtsZ (Unciuleac et al., 2016). FtsZ is a tubulin homolog polymerizes into a ring (Z-ring) at mid-cell to begin cell division. Suggesting cdc48 may play an essential role during cell division (Unciuleac et al., 2016).

In eukaryo and archaea Cdc48 forms complex with 20S proteasome and degraded ssrA-tagged substrates (Barthelme and Sauer, 2012). Not much is known about mycobacterial Cdc48 homologues but structural and biochemical characteristics of a Cdc48-like protein of actinobacteria (Cpa) has been described in *Msm*. In mycobacteria two proteins have been found to interact directly with the 20S proteasome, namely ARC (ATPase forming ring-shaped complexes), also referred to as Mpa (mycobacterial proteasomal ATPase) and a bacterial proteasome activator. These proteins act in an ATP-inde-pendent manner and are thought to aid in proteasomal degradation of proteins damaged under stress conditions, since they supports degradation of the unstructured model substrate casein and are involved in degradation of the conformationally unstable transcriptional heat shock protein repressor (Wu et al., 2017). In structural and biochemical study of MSMEG_0858 was shown to form a hexameric ring in the presence of nucleotides – correlating with ATPase activity.

The theory that MSMEG_0858 forms hexameric rings may also interact with the 20S proteasome was recently proven using a bacterial two-hybrid assay and electron microscopy (Figure 1.4) (Ziemski et al., 2018).

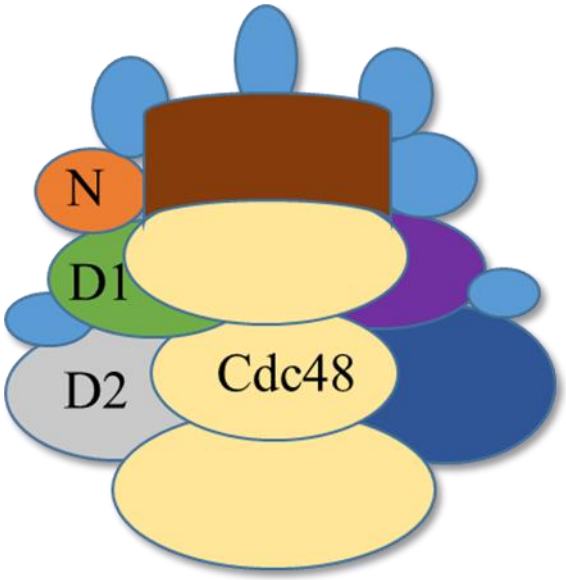

Figure 1.4 .Schematic representation of Hexameric state of cdc48. Show two domains 1 and 2 responsible for ATP hydrolysis and N-terminal. Hexameric ring of cdc48 can possible interact with 20s proteasome cytosol.

An *Msm* mutant strain lacking the *cdc48* gene exhibited growth defects under carbon starvation and the levels of several hundred proteins were altered more than 3-fold. Some of these proteins included those involved in transcription, energy production/conversion, amino acid metabolism/transport and lipid metabolism (Ziemski et al., 2018).

This suggested that MSMEG_0858 may play a role in adaptation to nutrient limitation. In addition, Cdc48 was thought to influence membrane stability since it was co-transcribed with *psd* and *pssA*, both of which are required for phosphatidylethanolamine synthesis. Phosphatidylethanolamine enables bacterial multi-drug transporters to function properly and facilitates the formation of intermediates required for the proper opening and closing of transporters (Ziemski et al., 2018). Deletion of Cdc48 from bacterial cells showed no significant

effect on cell division as there was no difference in cell size, length and morphology (Müller and Weber-Ban, 2019).

1.6 Study rationale

In the study by Poppy Mashilo (2018), MSMEG_0858 (*cdc48*) was found to interact with an essential low molecular weight penicillin binding protein DacB. Depletion of *dacB* was associated with alterations in peptidoglycan physiology (Ealand et al., 2019). In another study, a *Msm* strain lacking MSMEG_0858 showed growth defects under carbon starvation conditions and MSMEG_0858 had physical association with 20S proteasome (Ziemski et al., 2018). Therefore, MSMEG_0858 may play an important physiological role in cell division and cell wall maintenance (including peptidoglycan homeostasis; adaptation to nutrient deprivation; and response to cell wall or protein damaging agents).

1.7 Study hypothesis

MSMEG_0858 (Cdc48) interacts with DacB, an essential PG-associated enzyme, and therefore it plays a role in cell division and maintenance of cell wall integrity in *Msm.*

2 Aims and objectives

2.1 Aim

2.1.1 Phenotypically characterize the mutant strain lacking *cdc48* using novel PG probes (mono-peptide) to elucidate changes in PG biosynthesis and remodelling during growth in adverse (exposure to antibiotics) and nutrient limiting conditions.

2.2 Objectives

2.2.1 To confirm the genotypes of *Msm* wild-type, previously constructed Δ*cdc48* mutant and complemented (Δ*cdc48*::*cdc48*) strains.

2.2.2 To determine the growth kinetics of the wild-type, Δ*cdc48* mutant and complemented strains in nutrient rich media and carbon-starved conditions.

2.2.3 To assess the antibiotic susceptibility (MICs) of all strains to amoxicillin, D-cycloserine, streptomycin and vancomycin

2.2.4 To assess the susceptibility of all strains to cell wall and protein damaging agents (i.e. lysozyme and heat-shock/formaldehyde, respectively).

2.2.5 To assess the cell wall permeability of all strains.

2.2.6 To assess the effects of Cdc48 deletion on PG biosynthesis and remodelling by staining with PG-specific, mono-peptide fluorescent probes.

3 Materials and Methods

3.1 Chemicals and reagents used in this study

Reagents used for all media and chemical solution preparation were obtained from Sigma Aldrich and Thermo Fischer Scientific. All oligonucleotide primers were synthesized locally by Inqaba Biotechnical Industries Pty (Ltd). DNA restriction enzymes were either from Roche or New England BioLabs.

3.2 Bacterial strains used in this study

Table 1. Bacterial strains used in this study.

Bacterial strains	Description	Source
mc^{2}155	Efficient *Msm* ATTCC 607 transformation mutant.	Snapper et al., 1990
Δ*cdc48*	Derivative of mc^{2}155 carrying an unmarked, in-frame deletion in cdc48 (MSMEG_0858).	Poppy Mashilo, 2018
Δ*cdc48::cdc48*	Genetically complemented derivative of Δcdc48 carrying a full length copy of cdc48 plus the native promoter (200 bp upstream region) integrated at the attB site. Hygromycin resistance.	Poppy Mashilo, 2018

3.3 Bacterial strains culture conditions

All *Msm* strains were grown on Middlebrook 7H10 (19 g Difco Middlebrook 7H10, 5ml glycerol, 985 ml sdH2O)

solid media supplemented with 0.2 % glucose, 0.5 % glycerol, 0.085% NaCl, and appropriate antibiotics at 37 °C or in Middlebrook 7H9 (4.7 g Difco Middlebrook 7H9 powder, 2ml glycerol, 986 ml sdH2O) liquid media supplemented with 0.2% glucose, 0.085% NaCl, 0.5% glycerol, 0.05% Tween 80 and appropriate antibiotics at 37 °C with shaking at 100 rpm unless stated otherwise. Hygromycin was always used at a final concentration of 50 µg/ml (see supplementary Table A1 for media components).

3.3.1 Media composition for testing carbon-limitation

Pre-cultures (5 ml) were prepared by growing all *Msm* strains were grown in 7H9 (as described above) until the mid-exponential growth phase. Cells were then harvested by centrifugation at 4000 rpm for 10 min (4°C) and re-suspended in carbon-minimal media (containing 40 mM K_2HPO_4, 22 mM KH_2PO_4, 15 mM $(NH_4)_2SO_4$, 1.7 mM $Na_3C_6HSO_7$, 0.4mM $MgSO_4$, 0.05% Tween80). Glycerol was omitted from the media as it would have served as a carbon source. Hygromycin was added to the media in which the

complemented strain was cultured. All strains were then incubated at 37 °C with shaking at 100 rpm.

3.3.2 Extraction of genomic DNA for genotype confirmation

Two methods were used to isolate genomic DNA:

3.3.2.1 Small scale extraction (colony boil)

The colony boil method was used to extract chromosomal DNA from all *Msm* strains. Half a colony was scraped from solid, 7H10 media and re-suspended in 100 µl of sterile distilled water (sdH_2O). Tubes were then briefly vortexed prior to incubation at 95 °C for 5 min. One hundred microlitrers of chloroform was added to each tube which was then mixed vigorously for 5 – 10 s by vortexing. The suspension was then centrifuged at 12 470 × g for 5 min and the aqueous phase (containing nucleic acids) was transferred to a sterile 1.5 ml Eppendorf tube. Up to 3 µl was used as template in a PCR reaction.

3.3.2.2 Large scale extraction (CTAB method)

Mycobacterial strains were grown on 7H10 agar (as described above) until bacterial lawns were evident. Two to three loop-fulls of cells were scraped off the plate using sterile inoculation loops and re-suspended in 500 µl TE buffer (10 mM Tris- HCl, 10 mM EDTA, pH 8). Suspensions were then heat-killed at 65 °C for 30 min and snap-cooled on ice for 5 minutes. Following this, 70 µl lysozyme (10 mg/ml) was added and samples were further incubated at 37 °C for 1 hour. Thereafter, 6 µl of proteinase K (10 mg/ml) and 70 µl of 10 % SDS were mixed into the suspension and incubated for at least 2 hours (minimum of 30 min) at 65 °C. One hundred microlitrers of NaCl (5M) was added, followed by 80 µl of pre-warmed (65 °C) CTAB/NaCl (4.1% NaCl, 10% N – acetyl- N, N, N – trimethyl

ammonium bromide). The suspension was incubated at 65 °C for 10 min. An equal volume of chloroform:isoamyl alcohol (24:1, v/v) was added, mixed vigorously and centrifuged at 12 470 × g for 5 min at room temperature. The upper aqueous phase was then transferred into a sterile 1.5 ml Eppendorf tube.

The DNA was precipitated by addition of 600 µl isopropanol and centrifugation at 12 470 × g for 20 min. The pellet was then washed with 1 ml of 70 % ethanol by centrifugation at 12 470 × g for 3 min and vacuum-dried at 60 °C. Finally, DNA pellets were re-suspended in 150 µl of nuclease-free sdH_2O.

In order to purify genomic DNA samples, 1/10 volume (i.e. 15 µl) of 3 M sodium acetate was added to the DNA. Tubes were and mixed by inversion followed by the addition of 2.5 volumes (i.e. 330 µl) of 100% EtOH. Suspensions were then mixed by inversion and incubated at -20 °C for at least 30 min. Genomic DNA was then harvested by centrifugation at 12 470 × g for 20 min at room temperature and supernatant discarded. The DNA pellet was the washed with 0.5 ml of 70% EtOH and centrifuged at 12 470 × g for 5 min. The supernatant was discarded and pellet was vacuum-dried at 60 °C for 10 min. The DNA pellet was finally re-suspended in 50 µl sdH_2O and incubated at 65 °C for 10 min to facilitate complete re-suspension. Genomic DNA concentrations were determined by measuring 2 µl on a Nanodrop spectrophotometer (NanoDrop technologies). DNA concentrations were adjusted to ~ 25 ng/µl and if not immediately used in a PR reaction, stored at -20 °C until further use (see supplementary Table 1B and 1C for components of the solution used for DNA extraction and precipitation).

3.4 PCR confirmation of strain genotypes

Roche Faststart Taq DNA polymerase was used for all PCR analysis according to the manufacturer's instructions. Briefly, PCR reactions were set up using the following components:

5 µl of 10× recommended buffer, 10 µl 5× GC buffer, 2.5 µl of forward and reverse primer to a final concentration of 1 µM each, 8 µl of dNTPs to a final concentration of 0.2 µM, 2 U Taq polymerase, and 50 – 100 ng of genomic DNA as template. The final reaction volume was made up to 50 µl with nuclease-free sdH_2O. PCR reactions were incubated in a Bio-Rad (T100) thermal cycler using the following cycling conditions: 4 min of initial denaturation at 95 °C; 40 cycles of [95 °C for 15 sec, 45 s of annealing at 65 °C, 1 min of extension at 72 °C] and final extension step at 72 °C for 10 min.

3.5 Agarose gel electrophoresis for DNA visualization

Agarose gels were prepared by re-suspending 0.8 – 1 g of agarose (0.8 – 1%, w/v) in 1× TAE buffer (40 mM Tris-acetate, 1 mM EDTA). Agarose was completely dissolved by heating the suspension in a microwave until it boiled. Once sufficiently cooled (to ~ 60 °C), 2 µl of ethidium bromide (0.5 µg/ml) was added for every 50 ml. Samples (genomic DNA or PCR reactions) were loaded into the wells of the solidified agarose gel and electrophoresis was carried out in 1× TAE buffer at 80 – 100 V in electrophoresis tanks (Bio-Rab). DNA molecular weight markers (Roche) were separated on the same agarose gel to determine the molecular weight of the samples examined. Bands were then visualised using ultra-violet light in a G-Box system controlled by GeneSnap image acquisition software (Syngene) (see supplementary Table A4 and A5 for components of solution used for DNA electrophoresis and agarose gel recipe, respectively).

3.6 Southern hybridization for strain genotype confirmation

Genomic DNA was extracted (using the protocol of large-scale extraction described above) from all *Msm* strains. Approximately 3 µg of genomic DNA was digested with an appropriate restriction enzyme for one hour (incubation temperature dependent on restriction enzyme).

Briefly, reactions were set up in a 25 µl containing 1× appropriate restriction buffer, genomic DNA, 1 U restriction enzyme and sdH_2O.

Digested DNA was then separated using agarose gel electrophoresis [0.8 % agarose gel, w/v in 1× TAE buffer (242 g Tris base, 57.1 ml glacial acetic, 100 ml EDTA, pH 8)] at 90 V for 90 minutes and visualized using UV-light (Syngene G-BOX system).

Following this, the agarose gel was soaked in Depurination solution (1.5 M NaCl, 0.5 M NaOH) (Solution 1) for 15 min with shaking. Solution 1 was then discarded and the gel was rinsed twice with water. The gel was then soaked in Denaturation solution (Solution 2) at room temperature for 30 min with shaking. The gel was then neutralized by washing in 1X TBE buffer (100 ml 10 X Tris-Borate-EDTA, 900 ml sdH2O) A Hybond^{TM} Nitrocellulose membrane (Amersham Biosciences) was then placed over the agarose gel, sandwiched between two layers of Whatman filter paper and two layers of sponge. The entire setup was enclosed in a plastic cassette which was then transferred into an electro-blotting unit filled with 1X TBE buffer (100 ml 10 X Tris-Borate-EDTA, 900 ml sdH2O). The genomic DNA fragments in the agarose gel were transferred onto the nitrocellulose membrane at 600 mA and 130 V for 2 hours at 4 °C. Finally, the genomic DNA was cross-linked to the nitrocellulose membrane using ultra-violet light (UVC 500 Cross-linker, Amersham Biosciences) at 2500 mJ/cm3 for 2 min. Membranes were used immediately (if DIG-labelled probes were ready) or stored at 4 °C until use.

Regions (~1.5 kb) homologous to the upstream and downstream regions were PCR-amplified to create DIG-labelled probes for use in Southern hybridizations according to the manufacturer's instructions (PCR DIG Probe Synthesis Kit, Roche). This kit allows for specific labelling of probes by incorporating alkali-labile digoxygenin-labelled dUTP (DIG-dUTP) in place of dTTP into the sequence of the probe during a PCR amplification reaction. Incorporation of DIG dUTP into the probe sequence was confirmed by checking the PCR amplicons on 1 % agarose gel (as

described above). Successful labelling of the probe was detected by a shift (higher) in the molecular weight of the DNA fragment relative to its unlabelled counterpart. DIG-labelled probes were used immediately for hybridization or stored at – 20 °C until required.

If proceeding to hybridization immediately, the nitrocellulose membrane was pre-hybridized by placing the membrane into a Hybaid HB-OV-BM roller bottle (Thermo Scientific) containing 12 ml of DIG Easy Hyb solution (Roche) and incubated at ~55 °C for 30 – 120 min in a Hybaid Micro-4 hybridization oven (Thermo Scientific). The DIG-labelled probe was then denatured at 95 °C for 5 min and snapped-cooled on ice. The probe was then added to the membrane in the hybridization bottle and incubated overnight at ~55 °C whilst constantly turning. Following hybridization, the membrane was washed with Solution I [2× SSC (0.3 M Sodium citrate, 3 M NaCl) + 0.1% SDS] at the same temperature for 30 min before discarding. Twenty five millilitres of Solution 2 [0.5× SSC (0.3 M Sodium citrate, 3 M NaCl) + 0.1% SDS] were then added to the bottle which was further incubated at 68 °C for 15 min preparation for immunological detection of the DIG-labelled probe. Prior to immunological detection, the membrane was washed in a buffer (0.1 M Maleic Acid Buffer, 0.3% Tween20) at room temperature for 5 min and blocked in 1× blocking solution (10× blocking buffer, 1× maleic acid buffer) for 30 min. The membrane was then incubated in 20 ml anti-body solution (1: 10000 anti-DIG in 1X blocking solution) at room temperature for at least 30 min before washing twice with wash buffer (260 ml 1× maleic acid, 390 µl Tween 20). The membrane was equilibrated in 20 ml detection buffer (0.1 M Tris-Cl, 0.1 M NaCl, pH 9.5) for 5 min at room temperature and then placed into a hybridization bag (Roche) with the DNA side facing up. One millilitre of chloro-5-substituted adamantyl-1,2-dioxetane phosphate (CSPD) substrate was spread evenly over the membrane and incubated at 37 °C for 10 min. In a dark room, the membrane was exposed to X-ray films (CL-XposureTm Film, Thermo Scientific) for 30 min and then developed by incubation in developing solution, water, fixative

and then water (2 min per step). The film was left to air-dry and the probe signal (banding patterns) was compared to the expected sizes (see supplementary Table A6 for components of the solution used for southern blots analysis).

3.7 Assessment of mRNA transcript levels

Expression analysis of *cdc48*, *dacB* and *sigA* (house-keeping or reference gene) was conducted in four steps, namely: 1) total RNA isolation, 2) DNAse-treatment to remove residual genomic DNA, 3) cDNA synthesis and 4) qPCR analysis. Each will be described below.

3.7.1 Isolation of total RNA

Two different RNA extraction protocols were performed in to maximize the yield and quality of the RNA extracted. In the first method, a commercially available kit was used (Nucleospin RNA purification Kit, (Macherey-Nagel)) as per the manufacturer's instructions. Briefly, mycobacterial strains were grown in carbon-limited media to an OD_{600nm} ~ 0.6. Bacterial cells were harvested at 3 900 × g for 10 min at 4 ºC and the resultant pellets were re-suspended in 350 µl lysis buffer supplemented with 3.5 µl β-mercaptoethanol. The cell suspension was then transferred to Lysing matrix B tubes (IEPSA). Cells were disrupted in a Ribolyser (Roche) for 45 s (Speed = 6), with incubation on ice for 2 min between each cycle. The lysates were then cleared by passing through filters at 11 000 × g for 30 s. Thereafter, 350 µl of 70 % ethanol was added to the flow-through and the suspension transferred to nucleic acid binding columns. These were centrifuged at 11 000 × g for 30 s and the flow-through was discarded. A 350 µl aliquot of membrane desalting buffer (MBD) was added to the column, which was centrifuged at 11 000 × g for 30 s and the flow-though was discarded. An on-column DNAse-treatment was performed before washing and eluting the RNA in 50 µl volumes (using nuclease-free sdH_2O). The concentrations of RNA preparations were determined by measuring 2 µl on a NanoDrop spectrophotometer.

The second method used to isolated total RNA utilized the Tri-reagent. Mycobacterial cells at desired optically density (OD_{600nm} ~ 0.6) were centrifuged as above. Bacterial pellets were re-suspended in 1 ml of Tri-reagent and 4 µl of linear acrylamide (Amersham). The cell suspension was transferred to lysing matrix B tubes and lysed as above. Samples were centrifuged at 12 470 × *g* for 10 sec at room temperature to pellet cell debris and silica beads. Supernatants were transferred to sterile 2 ml Eppendorf tubes containing 300µl chloroform:isoamyl alcohol (24:1 v/v). The solution was mixed thoroughly by inverting rapidly and incubated at a room temperature for 2 min followed by centrifugation at 12 470 × g for 5 min. The upper aqueous layer was removed and transferred to a sterile 1.5ml Eppendorf tube. An equal volume of isopropanol was used to precipitate the RNA together with a 20 min centrifugation step and 12 470 × g. The RNA pellet was washed with 500 µl of 70% EtOH by inversion and centrifuged at 12 470 × g for 5 min. EtOH was carefully poured off and the pellet was vacuum-dried at 60 °C for 10 min. Finally, RNA was re-suspended in 40µl sdH_2O and incubated at 60 °C to facilitate the re-suspension.

Following extraction of total RNA with Tri-reagent, 260/280 and 260/230 ratios are typically low (< 1) and indicative of contaminants which inhibit cDNA synthesis. In order to circumvent this limitation, total RNA preparations were purified using butanol and diethylether (Krebs et al., 2009). Briefly, total RNA was mixed with 500 µl of saturated butanol (10ml dH_2O, 10ml butanol), briefly vortexed and then centrifuged for 5 sec to separate the phases. The upper, butanol phase was removed and discarded (wash step repeated for a minimum of 5 times). Residual butanol was removed by adding 500 µl of saturated diethylether (10ml diethylether, 10ml dH_2O) followed by vortexing and centrifugation as described above. Diethylether was then evaporated off the sample by incubating in a fume-hood for at least 30 min (wash step repeated twice). These wash procedures were repeated until the 260/280 and 260/230 ratios were greater than 1.5. Trizol method was preferred as it has high yields of RNA concentration and 260/230 ratio were greater

than 1 after purification. Extracted total RNA samples were then quantified using the Nanodrop and stored at – 80 °C until use.

3.7.2 DNAse-treatment of total RNA

One microgram of total RNA was mixed with 1× DNAse reaction buffer, 1U of DNAse and water (made up to a volume of 25 µl). Samples were briefly centrifuged to pool all the components and then incubated at 37 °C for 30 min. Another microlitre of DNAse was added to the tube and further incubated for 30 min. The DNAse reaction was inactivated by the addition of $1/10^{th}$ volume of inactivation agent (resin). Samples were mixed and then centrifuged at 12 470 × *g* for 5 min.

3.7.3 Synthesis of cDNA

RT-PCR (reverse-transcription PCR – creation of complementary DNA from mRNA) was performed using Superscript III reverse transcriptase [RT] (Invitrogen). Briefly, reactions were set up in 25 µl volumes containing ~23 µl of DNA free RNA (from step above, equivalent to ~ 1 µg of total RNA) and 2 µl reverse primer mix (final concentration = 2.5 µM) consisting of gene-specific primers (i.e. *sigA*, *dacB* and *cdc48*). Primers were annealed to the mRNA by incubation at 94 ºC for 90 s, 65 ºC for 3 min and 57 ºC for 3 min, followed by incubation on ice. The nucleic acid mix was then split into two equal volumes - one half for an RT reaction and the other to serve as an RT-free reaction control. In tubes containing RT, the following components were added: 5 µl 5 × first strand buffer, 4 µl of 25 mM $MgCl_2$, 2 µl of 0.1 mM Dithiothreitol (DTT), 1 µl of 10 mM dNTP mix and 0.5 µl Superscript III RT (SSIII). The RT free control contained the same components except SSIII (which was substituted by sdH_2O. Reactions were incubated at 50 ºC for 50 min, followed by heat inactivation of the RT enzyme at 85 ºC for 5 min. The cDNA (1 µl) was then used for qPCR.

3.7.4 Quantitative, real-time PCR (qPCR) analysis

Using either genomic DNA (as standards of known genome equivalents) or cDNA (prepared as above), qPCR reactions were performed using SYBR green chemistry (SsoFast Evergreen Supermix, Bio-Rad). In each case, 20 µl reactions (10 µl Supermix, 0.25 mM forwad primers, 0.25 mM reverse primers, 1 µl template). Reactions were incubated in a CFX96 Real-Time PCR thermal cycler (C1000, Bio-Rad) using the following parameters: enzyme activation step at 95 ºC for 30 sec, followed by 40 cycles consisting of 3 steps – denaturation at 95 ºC for 10 sec, annealing at 60 ºC for 10 sec and elongation at 72 ºC for 10 sec followed by a SYBR Green quantification. A melt curve (starting at 50 ºC and then gradually increasing by 0.5 ºC every 0.5 sec to 95 °C with a continuous SYBR Green quantification) was used to assess the specificity of the PCR reaction (i.e. one peak = one qPCR amplicon). Raw data was then processed using CFX Manager 2.1 software (Bio-Rad).

3.8 Phenotypic characterization of Msm strains (wild-type, Δcdc48 and Δcdc48::cdc48)

3.8.1 Growth kinetic analysis

The growth kinetics of each strain was determined in nutrient-rich (7H9 media supplemented with Tween80 glucose salts) and carbon-limited media. Pre-cultures were started from a freezer stock and grown overnight. Larger volumes (~25 ml) of media were inoculated to a starting OD_{600nm} = 0.05 (in triplicate). This time-point served as a "Time 0". Samples were incubated for 12 hours without sampling (this corresponded to the lag phase of growth). Thereafter, samples were removed every three hours to determine cell density (OD_{600nm}) and to prepare serial dilutions for CFU/ml calculations. Following plating of the dilutions (100 µl each) onto 7H10 media, plates were dried completely before incubation at 37 °C for 3 – 5 days. Colonies were manually scored to determine CFU/ml using the following formula:

*CFU/ml = (no. of colonies * dilution factor) / volume plated in ml*

3.8.2 Minimum inhibitory concentration (MIC) determination

The concentration of antibiotic required to inhibit the growth of various mycobacterial strains was determined using a micro-dilution assay. Briefly, bacterial strains were grown to an OD_{600nm} = 0.5. The micro-dilution plates were then set up using 96 well plates containing 12 rows. Antibiotic stocks, containing 4× the initial concentration required for the first row in the plate, were set up and 100 µl of the stock was inoculated into the first row. Thereafter, 50 µl of media was inoculated into rows 2 to 12, then a 50 µl aliquot of the antibiotic stock from row 1 was inoculated into row 2, mixed and 50 µl was removed from row 2 and inoculated into row 3. This was done through to row 12 and a 50 µl aliquot was removed from the last row and discarded. Bacterial cultures were diluted to an OD_{600nm} = 0.05 and a 50 µl aliquot was added to each well except row 1. Plates were sealed and incubated at 37 ˚C overnight without agitation. Alamar blue (Invitrogen) was added ($1/10^{th}$ volume = 10 µl) and plates were further incubated at 37 °C for 3 – 5 hours. Fluorescent signals (due to the conversion of Alamar blue from blue to pink) were measured on a plate reader (excitation and emission at 560 and 590 nm, respectively) to determine the MIC values each drug.

3.8.3 Ethidium bromide diffusion assay

Msm cells were grown to an OD_{600nm} ~ 0.8 in 7H9 media at 37 °C. Bacterial cultures were then centrifuged at 4 500 rpm for 10 minutes to harvest bacterial cells. The supernatant was discarded and the pellet was washed once in 1× PBS. The pellet was then re-suspended in 1× PBS containing and 0.4 % glucose. The OD_{600nm} was adjusted to 0.4 and 95 µl was added to a 96-well flat bottomed, black plate.

Ethidium bromide was added to a final concentration of 8 and 16 µg/ml in a total volume of 100 µl. The fluorescence (indicative of ethidium bromide bound to double-stranded DNA) was monitored at wavelengths of 530 nm and 585 nm (excitation and emission respectively) every 60 seconds for 60 minutes at 37 °C.

3.8.4 Heat shock and formaldehyde exposure assays

Msm strains were grown to an OD_{600nm} ~ 0.5 in 25 ml of 7H9 supplemented with glucose salts and Tween80. Cultures were divided into two equal volumes in sterile 50 ml falcon tubes. One tube was exposed to heat-shock (42 °C for 30 min) while the other was kept in a room temperature for the same amount of time. Appropriate serial dilutions were performed and 100 µl aliquots were plated on 7H10. Plates were allowed to dry completely before incubation at 37 °C for 3 – 5 days. Emergent colonies were then manually counted to determine CFUs/ml (using formula above) and to then determine the survival rate relative to untreated control samples for each stain.

The effects of exposure to formaldehyde (0.005%) were determined using a similar setup to that described above. All falcon tubes were incubated overnight at 37 °C with shaking (100 rpm). Following incubation, the OD_{600nm} of each culture was measured. Following this, formaldehyde was removed by centrifugation and bacterial pellets were re-suspended in the original volume (12.5 ml) of 7H9 media (unexposed strains were also centrifuged and re-suspended in 'fresh' 7H9 media for consistency). Appropriate serial dilutions were prepared and 100 µl of each was plated on 7H10 media for incubation and scoring (as above).

3.8.5 SDS recovery assay

Msm strains were grown to an OD_{600nm} ~ 0.5. 7H10 plates containing 0.001, 0.002 and 0.004% of SDS were prepared respectively. Plates without SDS served as a control (hygromycin supplemented plates were prepared for the complementation strain). A serial dilution of each

culture (prepared in triplicate) was performed and 10 µl of each aliquoted onto the respective plates (grids with blocks corresponding to different dilutions drawn on each plate). These were allowed to dry completely before incubation at 37 °C for 3 – 5 days. Emergent colonies were then manually scored to determine the level of SDS killing (i.e. survival score at each dilution).

3.8.6 Testing the effect of cdc48 deletion on PG metabolism (by virtue of supposed interaction with the LMW PBP, DacB)

Cells were grown until the time-point which corresponded with significant differences in growth rate between the Δcdc48 mutant and wild-type strains (as determined by the growth kinetics analysis (outlined in section 9.1). Cells were then harvested by centrifugation at 4000 rpm for 10 min at 4°C. Bacterial pellets were then re-suspended in 1 ml of 7H9 and split into two equal volumes (i.e. 500 µl). To one tube, 2.5 µl of BADA were added and incubated at 37 °C for 30 min. The other half served as an unlabelled (UL) control. After the staining period, cell suspensions were centrifuged at 12 470 × *g* to pellet the bacterial cells which were subsequently re-suspended in 100 µl of 2.5% of glutaraldehyde and incubated at room temperature for 30 min for fixation. To remove glutaraldehyde, cells suspensions were centrifuged at 12 470 × *g* and pellets were re-suspended in 50 µl 1X PBS. Ten microlitrers were spotted onto 2% agarose pads before viewing on a fluorescent microscope (using the bright-field and GFP channels – BADA excitation and emission at 405 and 512 nm, respectively; exposure time 1 sec).

4. Results

4.1 Confirmation of genotype of Msm wild-type, Δcdc48 and Δcdc48::cdc48 strains using PCR, Southern Hybridization and mRNA transcript analysis

In a previous study from our lab, an *Msm* mutant strain lacking the *cdc48* gene was generated using two-step allelic exchange by homologous recombination (Mashilo, 2018). The complemented derivative was then constructed by introducing a complementation vector (containing the wild-type cdc48 allele and the 200 bp upstream native cdc48 promoter region) into the Δ*cdc48* strain to generate the Δ*cdc48*::*cdc48 strain*. Before this phenotypic characterization of these strains could commence, the genotypes of all three were confirmed by PCR, Southern hybridization and quantitative real-time PCR (qPCR) (see supplementary Table B1, B2, B3 and B4 for primer DNA sequences used for confirmation of genotypes). The PCR screen was designed to use three primers (one forward [F1] and two reverse primers [R1 and R2]) (Figure 4.1A). The PCR screen was performed using different annealing temperatures to determine optimal temperature, which was found to be 65°C (see supplementary figure C1). The rationale for this was that the internal reverse primer [R1] would only anneal in the wild-type strain. When wild-type genomic DNA was used as template, an amplicon corresponding to the F1-R1 primer pair was observed (i.e 1370 bp). The bigger amplicon (i.e. 2537 bp corresponding to the F1-R2 primer pair) was not detected but this could be due to an insufficient extension time in the PCR temperature cycling profile. When gDNA from Δ*cdc48* strain was used, only one amplicon was observed (i.e. 493 bp from the F1-R2 primer pair). This proved that the *cdc48* gene had been truncated in this strain. Following complementation of the mutant strain, it was clear that a wild-type copy of the gene had been re-inserted into the genome since the corresponding amplicon (1370 bp, from the F1-R1 primer pair) was detected (Figure 4.1B). Primers were designed using mycobrowser.

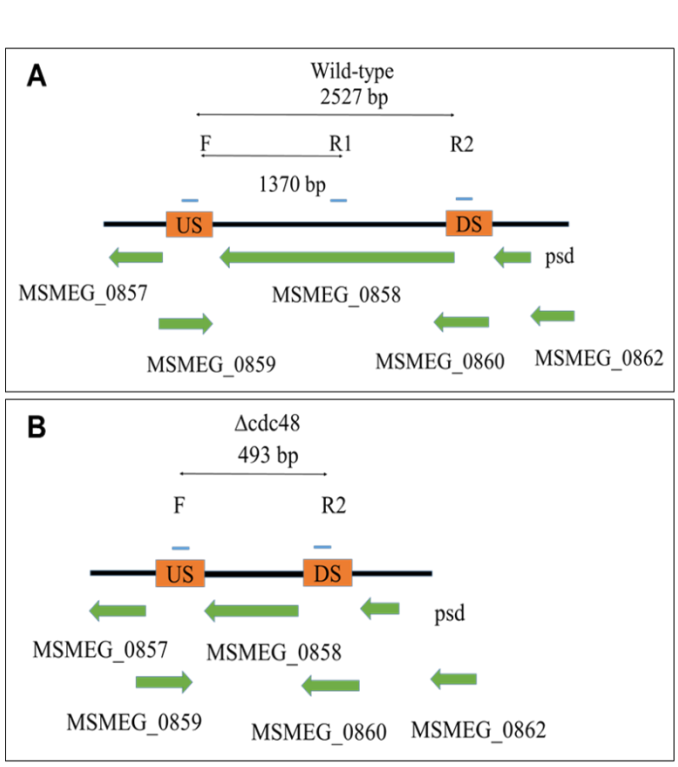

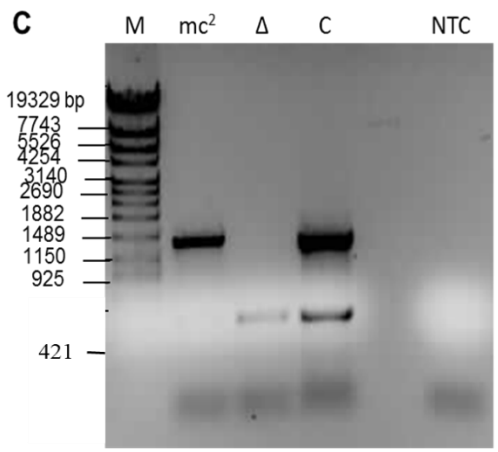

Strain	Expected amplicons when using all three screening primers (bp)
mc2155	2527, 1370
Δ*cdc48*	493
Δ*cdc48::cdc48*	1370, 493

Figure 4.1. Genotypic confirmation of wild-type and mutant strains. (A) Shows the genotypic context of MSMEG_0858 (*cdc48*) in the wild-type strain. Three primers – two flanking *cdc48* (F1 and R2) and one internal (R1). Orange boxes (US and DS) correspond to regions that were used to create the truncation in the deletion mutant strain (as in B). (C) PCR amplicons separated on a 1% TAE agarose gel. Fragments were sized using Molecular weight marker IV (Roche). Expected sizes were observed in the three strains tests and the no template control lane was empty (as expected).

Once the strains were confirmed by PCR analysis, it was necessary to show that the complementation vector had integrated into the expected site in the chromosome, i.e. *attB* phage attachment site. In addition, the expression level of *cdc48* in the complemented strain, relative to the wild-type mc^{2}155 strain, was also assessed. As seen in Figure 4.2B, PCR amplicons from both primer pairs corresponding to the expected sizes were detected in the complemented strain only. The absence of amplicons in the wild-type strain and no template control lanes suggested that the observed amplicons were specific and that complementation of Δ*cdc48* was successful.

All three strains were then grown to exponential phase to assess the transcript levels of *cdc48*. As seen in Figure 4.2C, *cdc48* was only detected in the wild-type and complemented strains. It is important to note that complementation was only partial because *cdc48* transcript levels only appeared to be half relative to the wild-type.

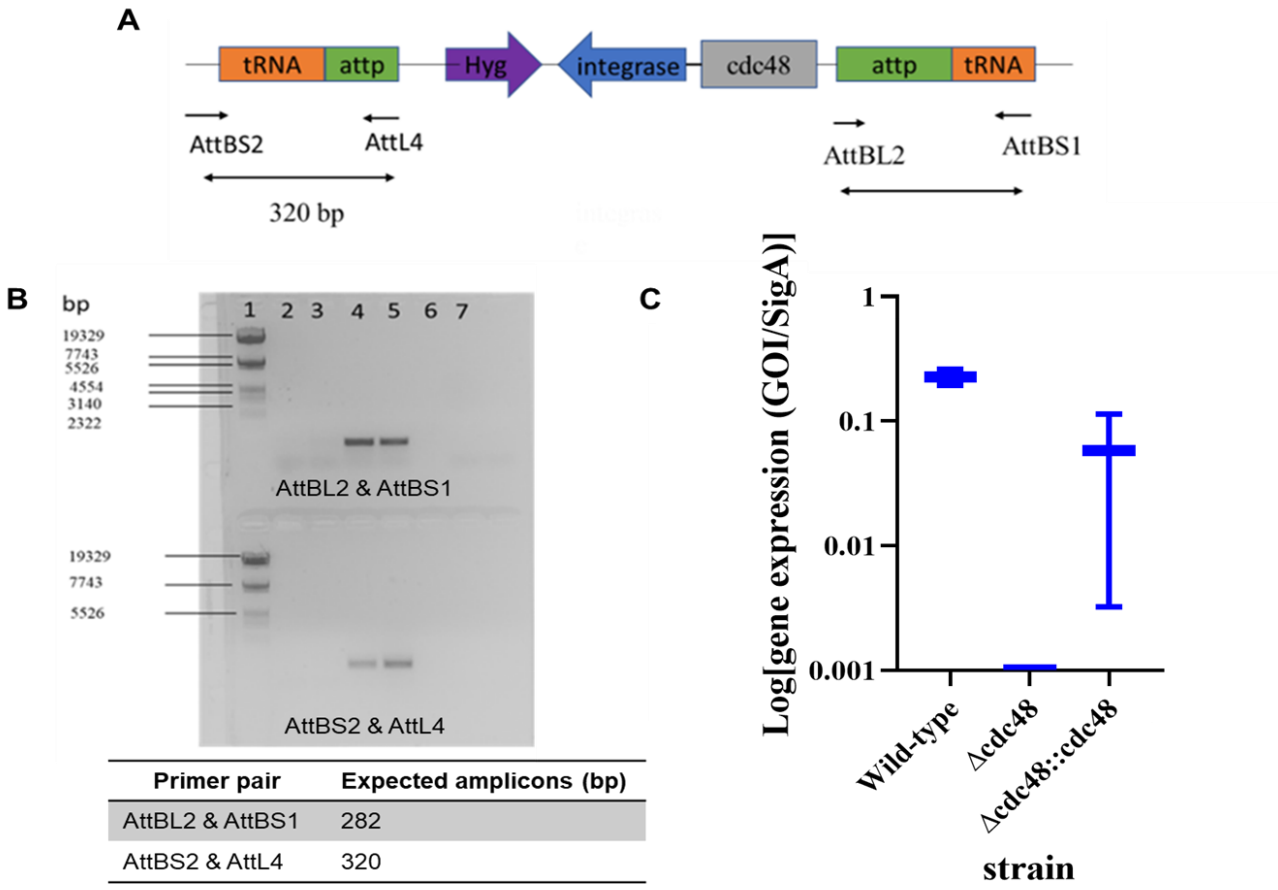

Primer pair	Expected amplicons (bp)
AttBL2 & AttBS1	282
AttBS2 & AttL4	320

Unpaired t-test	Mean Diff	95.00% CL of diff	Summary	P value
wild-type vs. Δcdc48	-0,1518 ± 0,07846	-0,3696 to 0,06605	ns	0,1252
wild-type vs. Δcdc48::cdc48	-0,1129 ± 0,08685	-0,3540 to 0,1282	ns	0,2635
Δcdc48 vs. Δcdc48::cdc48	-8,291 ± 6,338	-20,84 to 4,258	ns	0,3557

Figure 4.3. PCR confirmation of site-specific integration of pMV306*cdc48* into Δ*cdc48*. (A) Genomic context of the *attB* integration site after the incorporation in the complementation vector. The *attP* sites are derived from the plasmid DNA vector. Integration splits the *attB* site such that two primer pairs (i.e. AttBL2 & AttBS1 and AttBS2 & AttL4) can used to check for integration. (B) PCR amplicons checked on a 1% TAE agarose gel. [Top = AttL2 + AttBS1 primer set; Bottom = AttBS2 + AttL4 primer set]. Lane (1) Marker VI, lane (2-3) wild-type mc^2155, lane (4-5) complemented mutant strain, lane (6) empty, lane (7) no DNA control. Expected sizes shown in table below. (C) Expression levels of *cdc48* in mc^2155, Δ*cdc48* and Δ*cdc48::cdc48* were normalized by *sigA* levels. Data are representative of three independent biological repeats. Table shows results of an unpaired t-test for data in (C) (GraphPad Primer, Version 9). The data is non-significant p-value > 0.05 (Figure 4.3C).

The final test to confirm that the strains were correct was to perform a Southern blot. Genomic DNA from each was digested with *Bam*HI and transferred to a nitro-cellulose membrane (Supplementary Figure C5). Initially, two DIG-labelled probes were synthesized using PCR – corresponding to the upstream (US) and downstream (DS) regions of *cdc48*. Successful labelling of the probe was determined by comparing labelled (HOT) and unlabelled (COLD) reactions. When the amplicons were checked on an agarose gel, it was evident that the HOT reactions contained amplicons of slightly higher molecular weights which was indicative of DIG-label incorporation (Supplementary Figure C4). Only the US probe worked because several non-specific amplicons were observed for the DS probe (Supplementary Figure C3). As a result, only the US probe was used for subsequent Southern hybridizations. The expected fragments (3334 and 2495 bp) were observed in the wild-type strain (Figure 4.4D). Due to the truncation of *cdc48* in the genome, the smaller, expected size for one of the fragments (3334 and 495 bp) was observed in Δ*cdc48*. Lastly, the expected banding patterns for Δ*cdc48::cdc48* were calculated due to the presence of the integrated complementation vector (Figure 4.3). Due to a homologous region in the full-length gene, the probe correctly detected three DNA fragments, i.e. 3334, 2404

and 461 bp. Taken together, three independent molecular techniques have confirmed the genotypes for each strain used in the study.

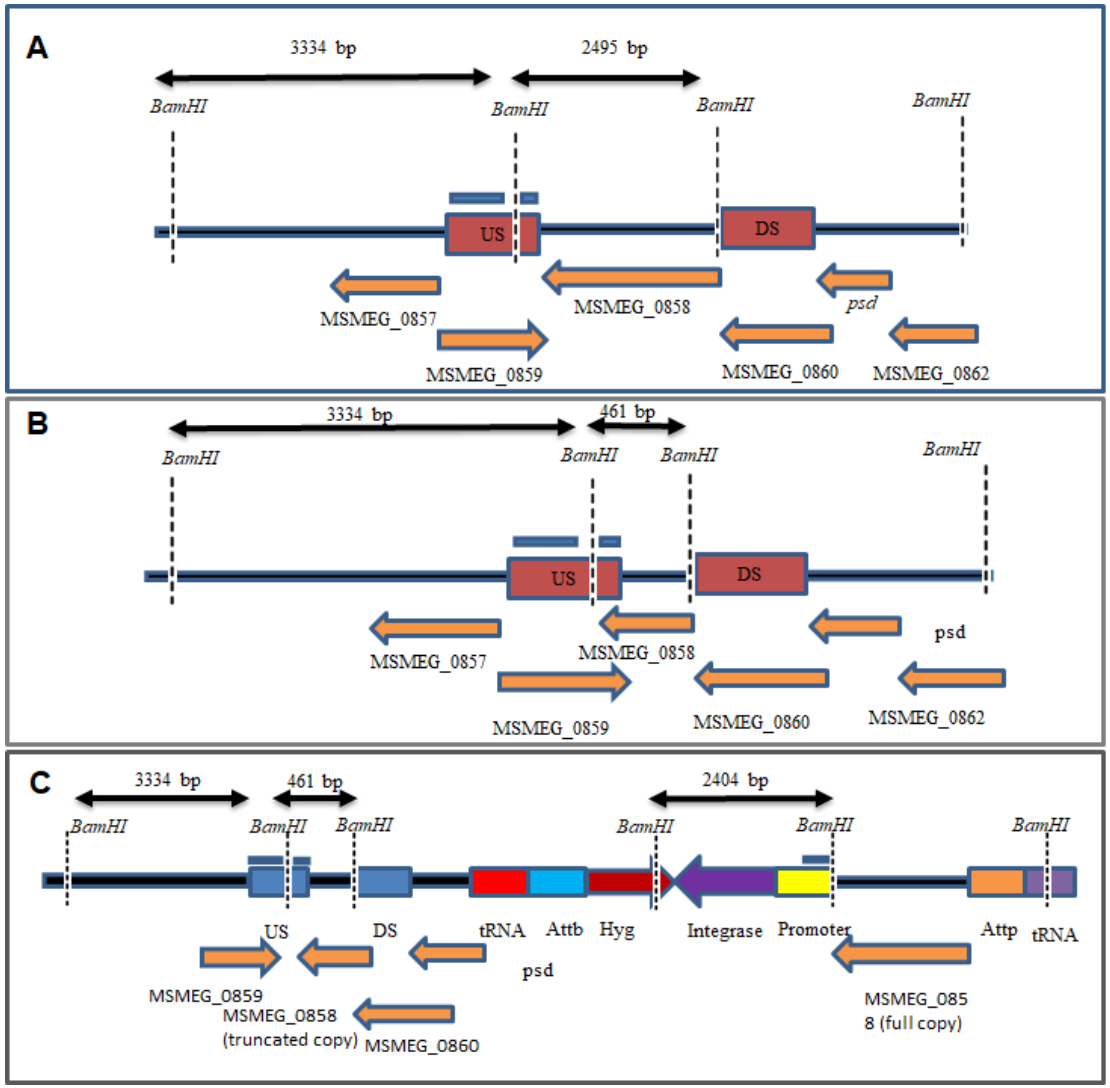

D

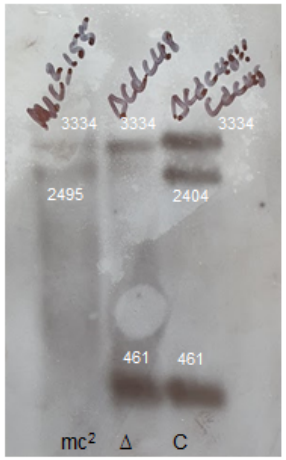

Strains	Expected size fragments (bp)
mc²155	3334 and 2495
Δ*cdc48*	3334 and 461
Δ*cdc48::cdc48*	3334, 461 and 2404

Figure 4.4. Southern blot hybridization to confirm wild-type and mutant strains. Genomic DNA (~3 µg) was digested with *Bam*HI for wild-type, Δ*cdc48* and Δ*cdc48::cdc48*. Genomic context for each shown in (A), (B) and (C), respectively. Following transferral of the DNA fragments to a nitro-cellulose membrane, a DIG-labelled probe (corresponding to the US region of *cdc48*) was used. (D) A Southern hybridization detected DNA fragments of the expected sizes in each of the strains.

4.2 Phenotypic characterization of Δ*cdc48*

To determine the biological role of Cdc48 in cell division and survival under adverse experimental conditions, different assays were performed. In each case, the wild-type (mc^2155) and complemented (Δ*cdc48::cdc48*) strains served as controls. Tests included:

(i) the analyses of growth kinetics

(ii) assessment of incorporation and remodelling of newly synthesized PG using PG-specific probes - by virtue of the supposed interaction of *cdc48* with the PG-associated enzyme *dacB*,

(iii) assessment of cell wall permeability

(iv) determination of sensitivity to protein and/or cell-wall targeting agents

4.2.1 Determination of growth kinetics

To evaluate the role of Cdc48 in regulating *Msm* growth kinetics, growth analyses were carried out on the wildtype mc^2155, the *Δcdc48* mutant and the complemented derivative strains. Growth kinetics were determined by the use of growth curves conducted in triplicate and growth assays were set up as described in section 3.3 and 3.3.1. As observed in Figure 4.5A the graph on the left, deletion of *cdc48* had no significant effect on *Msm* when cultured in 7H9 media. Both cell density (OD_{600nm}) and culturability (CFU/ml) in all strains were indistinguishable – the OD_{600nm} of the Δ*cdc48::cdc48* was slightly less than the other two strains but this was not evident in the CFU/ml data Figure 4.5B graph on the left.

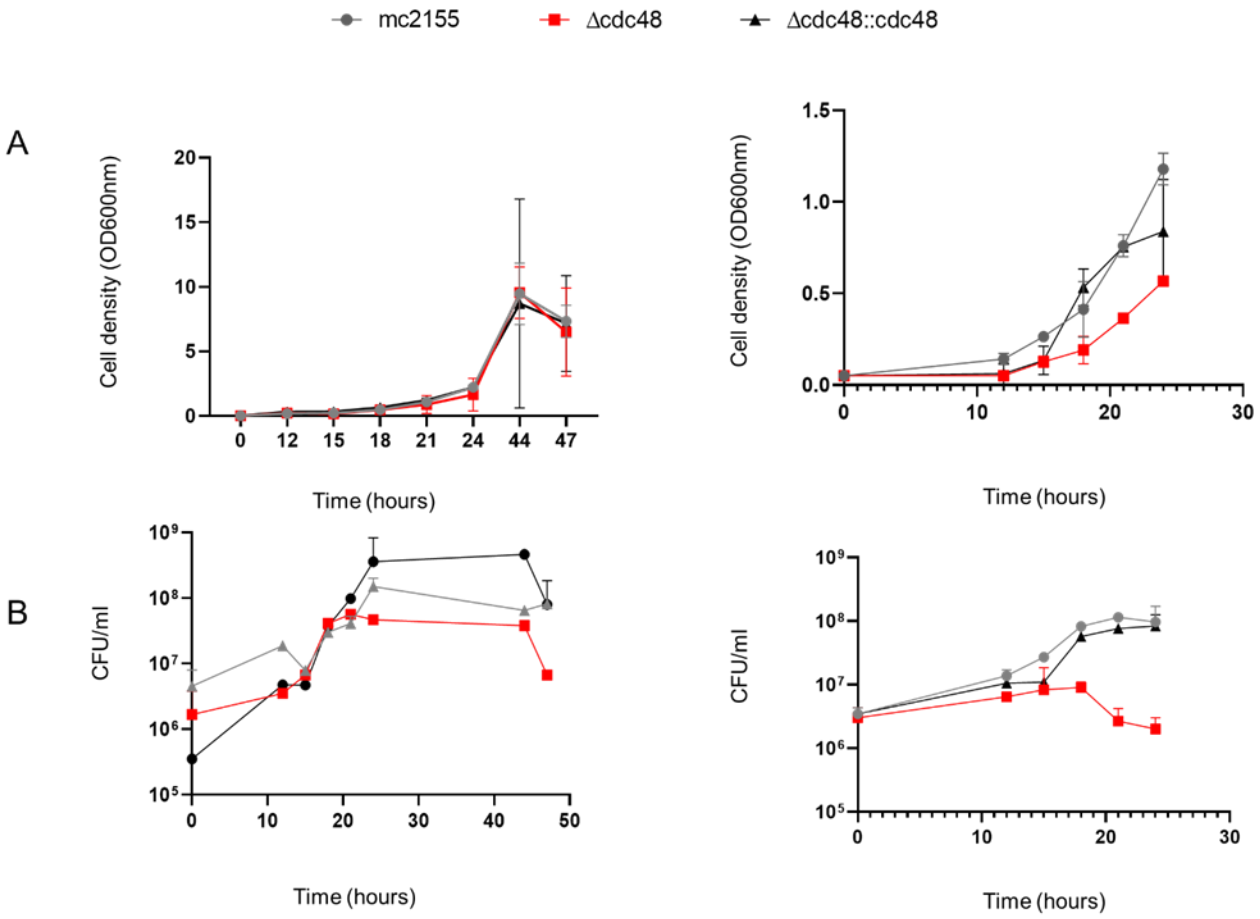

	Unpaired t-test	Mean Diff	95.00% CL of diff	Summary	P value
7H9 media	**wild-type vs. Δcdc48**	-4,086 to 3,696	-0,1948 ± 1,814	ns	0,9160
	wild-type vs. Δcdc48::cdc48	-0,04746 ± 1,770	-3,844 to 3,749	ns	0,9790
	Δcdc48 vs. Δcdc48::cdc48	0,1473 ± 1,747	-3,599 to 3,893	ns	0,9340
Carbon starvation	**wild-type vs. Δcdc48**	-0,2436 ± 0,1937	-0,6753 to 0,1880	ns	0,2372
	wild-type vs. Δcdc48::cdc48	-0,07282 ± 0,2281	-0,5810 to 0,4353	ns	0,7561
	Δcdc48 vs. Δcdc48::cdc48	0,1708 ± 0,1684	-0,2044 to 0,5460	ns	0,3344

Figure 4.5. Growth kinetics of the Δ*cdc48* strain relative to the wild-type (mc²155) and complemented (Δ*cdc48::cdc48*) strains. Growth curves were constructed by measuring the increase in optical density (OD600nm) and CFU/ml of the cultures at three hour intervals. (A) Growth measured in cell density in a nutrient-rich 7H9 media

versus in modified minimum media containing no glycerol. (B) Growth measured in CFU/ml in a nutrient-rich 7H9 media versus in modified minimum media containing no glycerol. Data are represent the means and standard errors from three independent biological replicates. Table shows results of an unpaired t-test (GraphPad Primer, Version 9). The data is non-significant p-value > 0.05 for both 7H9 media and minimum media with no glycerol.

In contrast, when the Δ*cdc48* strain was cultured under carbon starvation conditions, it grew slower than the wild-type strain. This phenotype was reversed following complementation with the full-length gene. By 18 hours post inoculation, Δ*cdc48* already displayed a lower cell density and this correlated with a lower concentration of culturable bacteria Figure 4.5A the graph on right and CFUs were lower when compared to wildtype Figure 4B the graph on the right. This result was not novel in that a previous study observed a similar result for an *Msm* strain lacking (MSMEG_0858 or Cpa) (Ziemski *et al*., 2018). In addition, the same study, a when the wild-type and Cpa knockout strain were grown under carbon starvation, significant changes in the concentrations of approximately 500 different proteins were observed. Since this study was interested the interaction of Cdc48 (Cpa) with DacB, it was possible that DacB was one of the 500 proteins altered under carbon starvation conditions. In order to test this hypothesis, independent cultures for each strain (performed in triplicate) were grown in carbon starvation media for 24 hours – equivalent to the greatest difference in cell density and CFU/ml (Figure 4.5B) – and cells harvested for gene expression analysis of *cdc48* and *dacB*. As observed in Figure 4.6, the deletion of *cdc48* had no effect on the expression of *dacB* suggesting either that any phenotypic differences were small or that a PG-specific test (to probe DacB) was required. This rationale was based on the observation of Ealand et al (2019) in which alterations in the levels of DacB resulted in a reduction of bi-polar growth with a corresponding increase in mono-polar growth. Table 2 shows the concentration on RNA extracted using MN kit and trizol method.

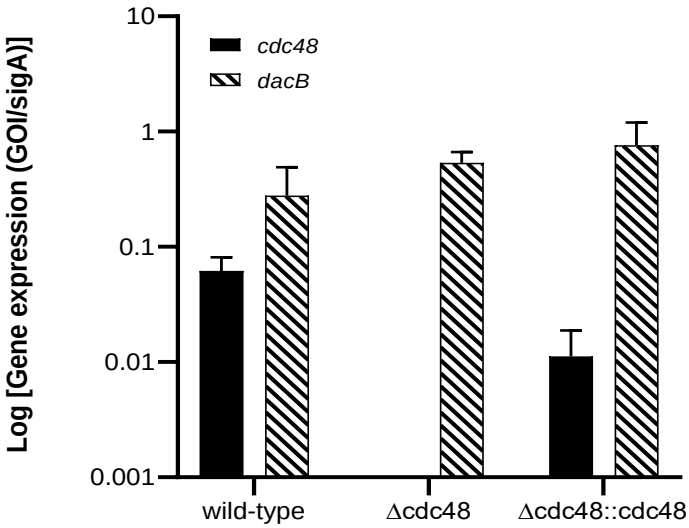

Gene expression comparison	Unpaired t-test	Mean Diff	95.00% CL of diff	Summary	P value
dacB	**wild-type vs. Δcdc48**	0,3497 ± 0,1473	-0,05931 to 0,7586	ns	0,0765
	wild-type vs. Δcdc48::cdc48	0,5733 ± 0,2842	-0,2157 to 1,362	ns	0,1138
	Δcdc48 vs. Δcdc48::cdc48	0,2237 ± 0,2651	-0,5124 to 0,9597	ns	0,4464

Figure 4.6. Transcript expression analysis of *cdc48* and *dacB* under carbon starvation conditions. Transcript levels (for *cdc48* and *dacB*) were assessed in axenic cultures after strains were grown in carbon starvation media for 24 hours. Data represent the average of the results from three independent biological repeats. A one-way analysis of variance (ANOVA) detected no statistically significance differences in the gene expression patterns of *dacB* in the various strains tested. Table shows results of an unpaired t-test (GraphPad Primer, Version 9). The data is non-significant p-value > 0.05 for dacB expression comparison across the strains.

Table 2. Comparison of RNA extractions using MN kit and Trizol method. RNA concentrations (ng/µl) and purity (260/230 ratios) after extraction using different methods.

	MN kit		Trizol	
Sample	**RNA concentration (µg/ml)**	**260/230 ratio**	**RNA concentration**	**260/230 ratio**
mc²155 (sample1)	8.68	0.11	468.55	1.31
mc²155 (sample 2)	4.47	0.12	568.55	1.29
mc²155 (sample3	9.16	0.11	532.12	1.40
Δ*cdc48* (sample 1)	12.24	0.14	1977.56	1.54
Δ*cdc48* (sample2)	9.11	0.15	1587.49	0.90
Δ*cdc48* (sample3)	596.93	2.06	1142.97	0.90
Δ*cdc48:cdc48* (sample1)	38.70	0.40	936.07	0.84
Δ*cdc48:cdc48* (sample2)	6.70	0.14	176.43	0.52
Δ*cdc48::cdc48* (sample3)	13.20	0.36	760.03	0.54

4.2.2 Interrogation of PG staining patterns in the Δcdc48 strain as a probe for alterations in dacB function

Using the same bacterial cultures (from which mRNA transcript analysis data were derived), cells were removed at 24 hours and stained with the PG-specific mono-peptide probe BADA. In these experiments, the cell-lengths for the wild-type and mutant strains, as well as the uptake of the BADA stain, were determined. Deletion of *cdc48* did not have a statistically significant effect on cell-length (Figure 4.7, insert). This was surprising in the context of the slower growth rate observed for Δ*cdc48* (see Figure 4.5B). The staining patterns or BADA uptake was further interrogated to determine whether PG biosynthesis was altered. Mycobacterial species adopt a growth pattern characterized by bi-polar extension (Aldridge et al., 2012, Joyce et al., 2012, Singh et al., 2013, Brown et al., 2011, Melzer et al., 2018). Each strain was subsequently scored for the following PG-staining patterns – mono-polar; bipolar; septa only; poles + septa; uniform staining across the entire cell and multi-septa (Figure 4.7 and Figure 4.8). As expected, cells in the wild-type population displayed a pre-dominant bi-polar staining pattern (~ 30%) with a lower frequency of cells stained only at a single pole (~ 20%). Cells containing one septa, stained poles & septa, uniform staining of the entire cell and multiple septa were relatively low (all below

20%). In contrast, Δ*cdc48* displayed a low frequency of unipolar or bipolar growth (both below 10%) but a much higher frequency of cell containing septa (~40%). In addition, this cells in this mutant population also contained more cells with multiple septa (~15%) relative to the wild-type (~5%). These data suggested that deletion of *cdc48* affects cell division in *Msm*. Assessment of these staining patterns in Δ*cdc48::cdc48* suggested that complementation did not restore the wild-type phenotype but this was not surprising since the mRNA transcript analysis in Figure 4.3C suggested that approximately 30% of the *cdc48* levels were detected following complementation with the full-length gene and its native promoter (relative to the wild-type strain).

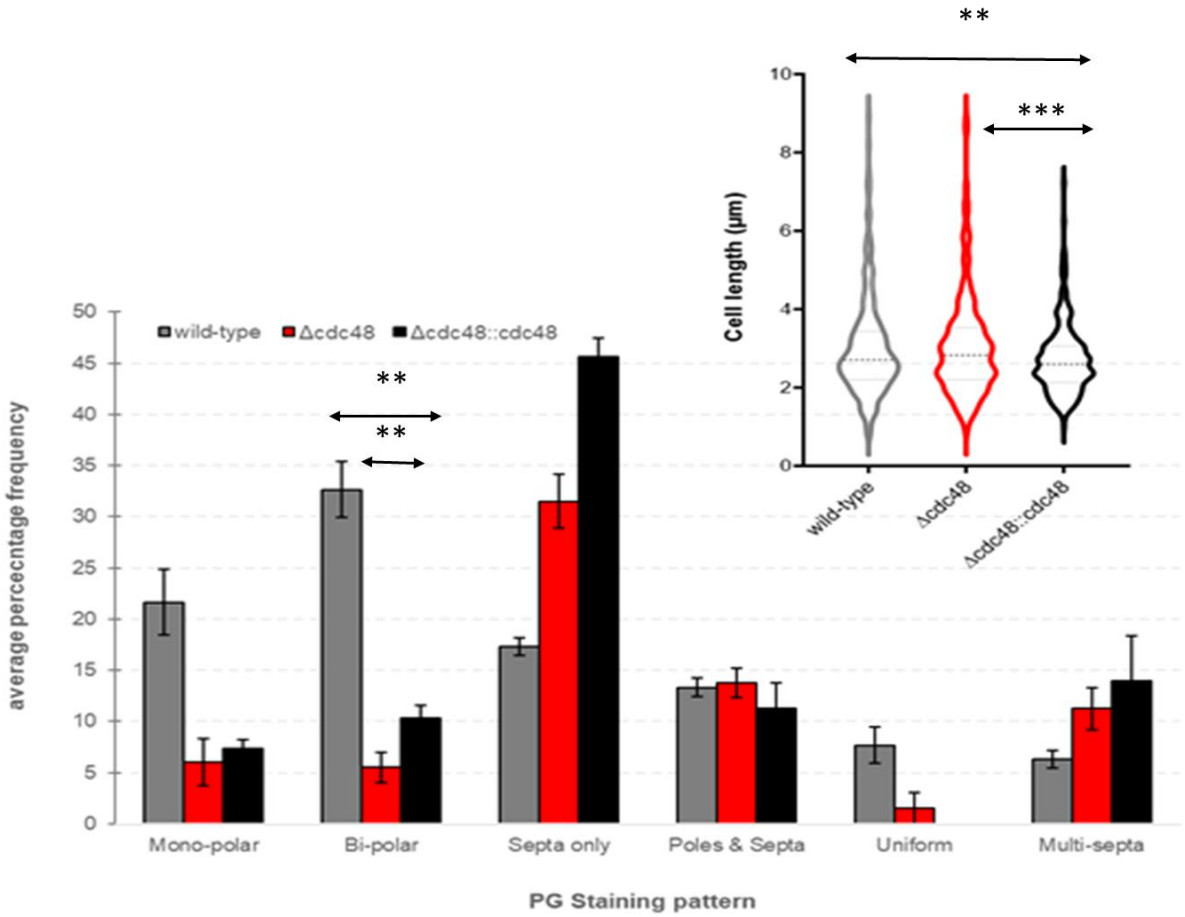

	Unpaired t-test	Mean Diff	95.00% CL of diff	Summary	P value
Cell length (µm)	**wild-type vs. Δcdc48**	0,04178 ± 0,1046	-0,1637 to 0,2472	ns	0,6897
	wild-type vs. Δcdc48::cdc48	-0,2825 ± 0,08823	-0,4557 to -0,1092	**	0,0014
	Δcdc48 vs. Δcdc48::cdc48	-0,3242 ± 0,09022	-0,5014 to -0,1471	***	0,0004
BADA PG staining pattern comparison Bipolar	**wild-type vs. Δcdc48**	-25,33 ± 3,091	-33,92 to -16,75	**	0,0012
	wild-type vs. Δcdc48::cdc48	-22,33 ± 2,981	-30,61 to -14,06	**	0,0017
	Δcdc48 vs. Δcdc48::cdc48	3,000 ± 1,886	-2,235 to 8,235	ns	0,1868

Figure 4.7. Cell length and BADA-uptake patterns in wild-type and mutant strains. Each of the strains were grown for 24 hours in carbon-starvation media – corresponding to the most significant differences in growth rate between strains (see Figure 4.5B). One millilitre aliquots were removed and split equally. To one aliquot, 2.5 µl of BADA was added while the other served as an unlabelled control. Both tubes were incubated at 37 °C for 30 min before fixing in 2.5% glutaraldehyde. After fixing, cells were re-suspended in 50 µl 1X PBS before spotting 10 µl onto a 2% agarose pad. Cells were then viewed using a fluorescent microscope in two channels (i.e. bright-field and GFP). Cell lengths and BADA-staining patterns were determined for at least 100 cells in each of the three biological repeats. 100 cells per replicate were captured with microscope. For each replicate cells imageJ software was used to determine the cell length of the cells and the data was plotted on the graphpad. Also for PG pattern analysis number of cells were counted in total of 100 cells showing different PG staining pattern and that number was multiply by 100 per replicate. Percentage frequency = (number of cells counted for particular PG pattern/total number of cells counted) × 100. Table above shows results of an unpaired t-test (GraphPad Primer, Version 9). Steric (*) sign show there was significance difference as the p-value < 0.05.

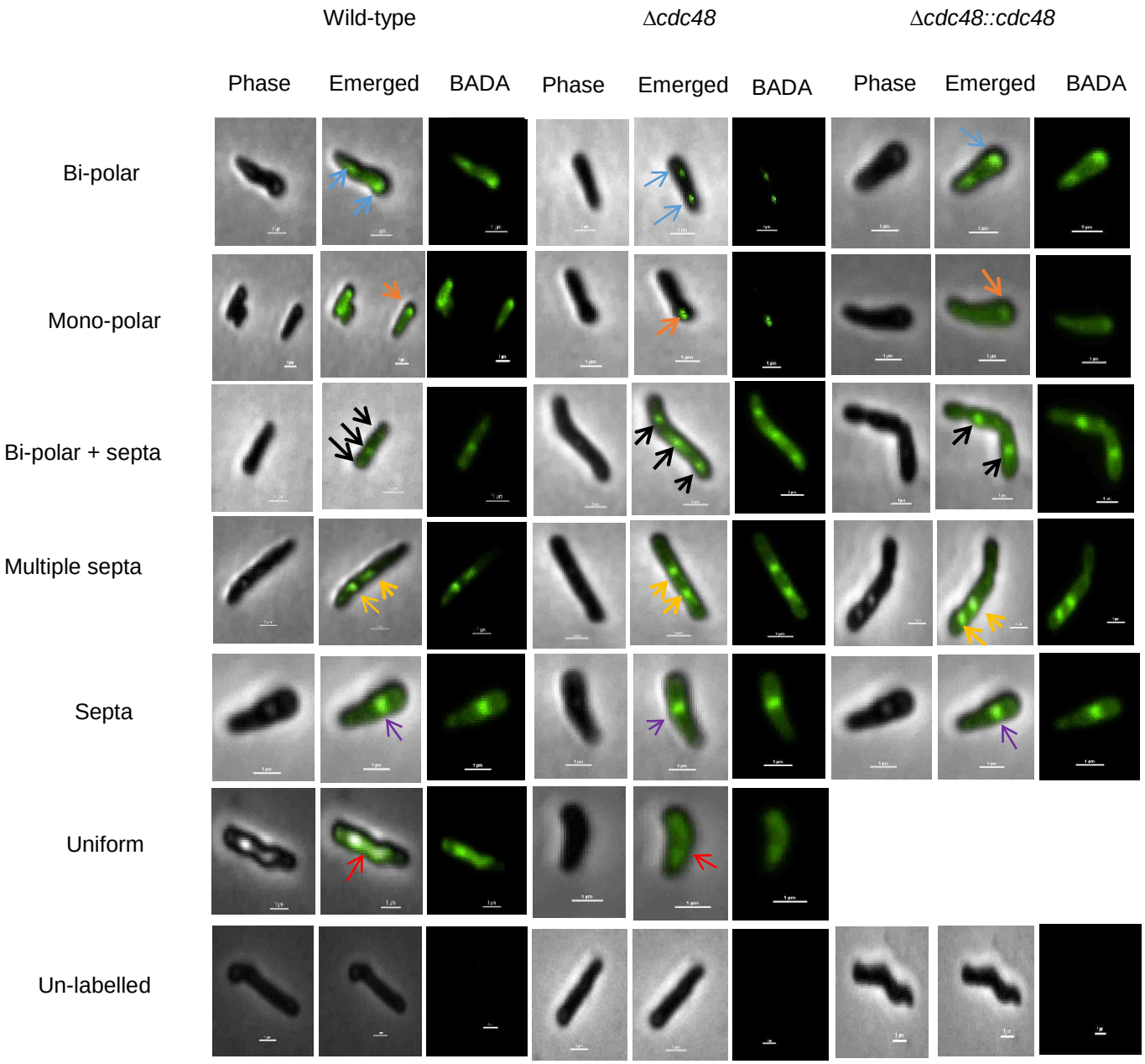

Figure 4.8. PG staining of cell wall with FDAA (fluorescent D-amino acid) BADA. Images above shows the incorporation of new synthesized PG on different sites in carbon starved *Msm* cells. Arrows shows different PG staining pattern: Blue arrows-bipole sites, orange arrow -unipole , black arrows – bipole +septa, yellow arrows – multiple septa, purple arrow – septa, red arrow – uniform. Scale bar used is 1µm. Experiment was done in triplicate and 100 cells were counted. Parameters for BADA are as follows excitation =405nm, emission=512nm and auto exposure 1s.

4.2.2 Assessment of cell wall permeability

Considering that PG biosynthesis and remodelling patterns were altered as a result of *cdc48* deletion, it was thought that cell permeability may be adversely affected. To test this, an ethidium bromide (EtBr) uptake assay was used. EtBr is able to passively cross the bacterial cell wall and membrane where it binds to the double-stranded, genomic DNA. This binding is emits a fluorescent signal which can be quantified. As observed in Figure 4.9, EtBr was able to penetrate the cell wall of Δ*cdc48* more relative to the wild-type and Δ*cdc48::cdc48* strains (P<0.0001). Complementation with the full length *cdc48* only partially reversed this phenotype as the differences in EtBr uptake for the Δ*cdc48::cdc48* strain remained statistically significant relative to the wild-type.

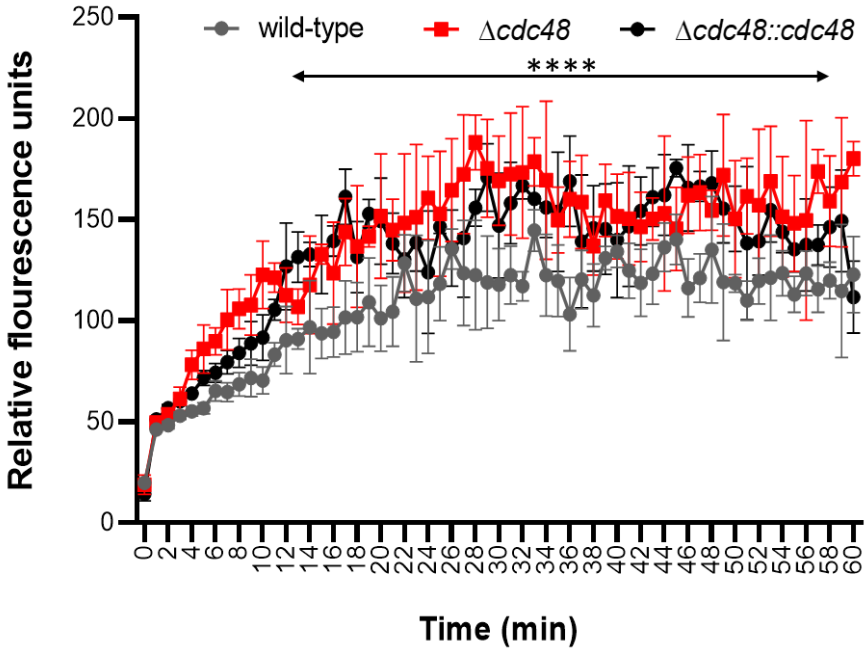

Unpaired t-test	Mean Diff	95.00% CL of diff	Summary	P value
wild-type vs. Δcdc48	34,87 ± 5,672	23,63 to 46,10	****	<0.0001
wild-type vs. Δcdc48::cdc48	26,57 ± 5,631	15,42 to 37,72	****	<0.0001
Δcdc48 vs. Δcdc48::cdc48	-8,291 ± 6,338	-20,84 to 4,258	Ns	0.1933

Figure 4.9. EtBr uptake increases as a result of *cdc48* deletion. Cell wall permeability of each strain was monitored by quantifying accumulation of EtBr (8 µg/ml) into the cells over time. Data are representative of three independent biological repeats whereas error bars represent the standard error of the mean. Table above shows results of an unpaired t-test (GraphPad Primer, Version 9). Steric (*) sign shows there was significance difference as the p-value < 0.05.

4.2.3 Determination of sensitivity to protein and/or cell-wall targeting agents

In addition to determining the increased cell wall permeability of the Δcdc48 strain, we investigated whether there would be an associated increase in the susceptibility to various drugs targeting PG biosynthesis (including amoxicillin, vancomycin, D-cycloserine), protein homeostasis (formaldehyde) and other factors that damage the cell wall and proteins (e.g. lysozyme, SDS and heat shock). For all antibiotics, lysozyme and formaldehyde, minimum inhibitory concentrations (MICs) for the compounds were assessed using the micro-broth dilution method. The parental mc2155 strain served as the reference. The MIC is defined as the minimum antibiotic concentration that results in growth inhibition. Drugs targeting the PG component of the cell wall were not more effective at killing the Δ*cdc48* strain. Compared to the wild-type and Δ*cdc48::cdc48* strains, the MIC50 values for amoxicillin, vancomycin and DCS were approximately 62.5, 2 and 15.6 µg/ml, respectively. Similarly, enzymatic damage to the cell wall (via lysozyme) failed to enhance killing in Δ*cdc48* – all strains had an MIC_{50} ~ 39 µg/ml (Figure 4.10C).

In order to investigate the role of *cdc48* in tolerating protein synthesis/damage, a few approaches were tested – including exposure to streptomycin, formaldehyde, heat shock and SDS. In the case of streptomycin and formaldehyde, an MIC_{50} was established as described above. In the wild-type strain, the MIC_{50} for streptomycin was 0.5 µg/ml which was the same for and Δ*cdc48* and Δ*cdc48::cdc48* (Figure 4.10A). Similarly, exposure to formaldehyde was not associated with an increased susceptibility in Δ*cdc48* as all three strains had an MIC_{50} between 0.0039 and 0.0078%

(Figure 4.11B). To explore this further, exposure to a sub-minimal concentration of formaldehyde (0.0015%) was tested. After exposure, all three strains survived equally (~10^7 CFU/ml) relative to the untreated controls.

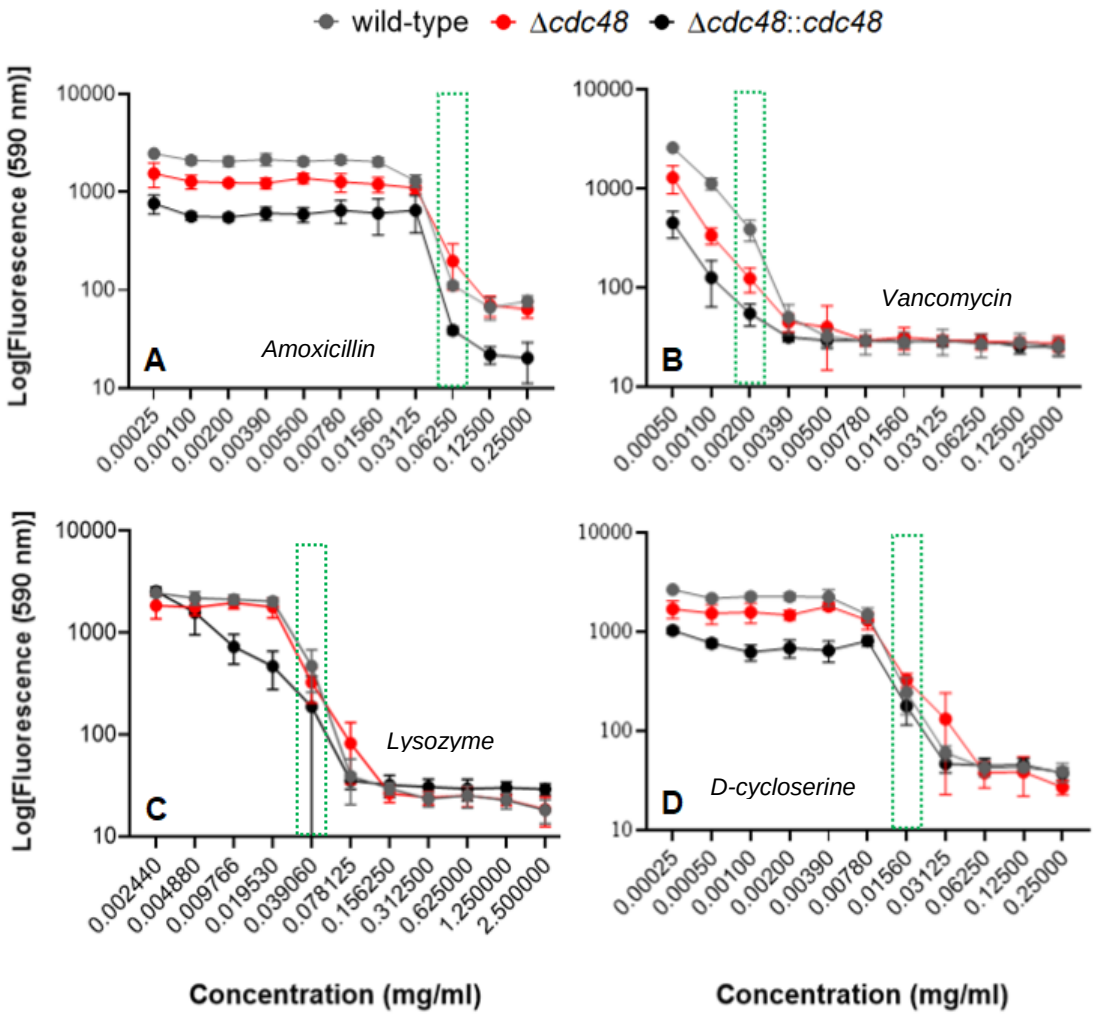

Figure 4.10. Determination of MICs for antibiotics targeting the PG component of the mycobacterial cell wall. Strains were grown to mid-exponential phase and the diluted appropriately. A starting concentration of 1 mg/ml for each drug (**A** – amoxicillin; **B** – vancomycin; **C** – lysozyme and **D** – D-cycloserine) was serially diluted across a 96-well, round-bottom plate. Each strain was added to each well (except for first row which served as a control) and incubated overnight (≥16 hours) at 37 °C without shaking. Following incubation, 10 µl Alamar blue (1/10th well volume) was added and further incubated at 37 °C for 3 – 5 hours. Conversion of resazurin (Alamar blue) occurs in response to cellular metabolic reduction and is accompanied by a change from blue to fluorescent pink (only viable cells can reduce the compound). Fluorescence was quantitated in a plate reader (excitation of 530-560nm and

emission of 590nm). One plate was used per strain which included media and diluent controls. Data are representative of the mean for six independent repeats and error bars reflect the standard error from the mean (SEM). **Green boxes** represent approximate MIC_{50} for each drug. See supplementary figure C6, C7, C8 and C9 for MICs plates used to determine MICs value for amoxicillin, vancomycin, lysozyme and D-cycloserine. The MICs value for antibiotics were non-significance difference as the fold MIC fluorescence was less than 2 and this was supported by MICs plate

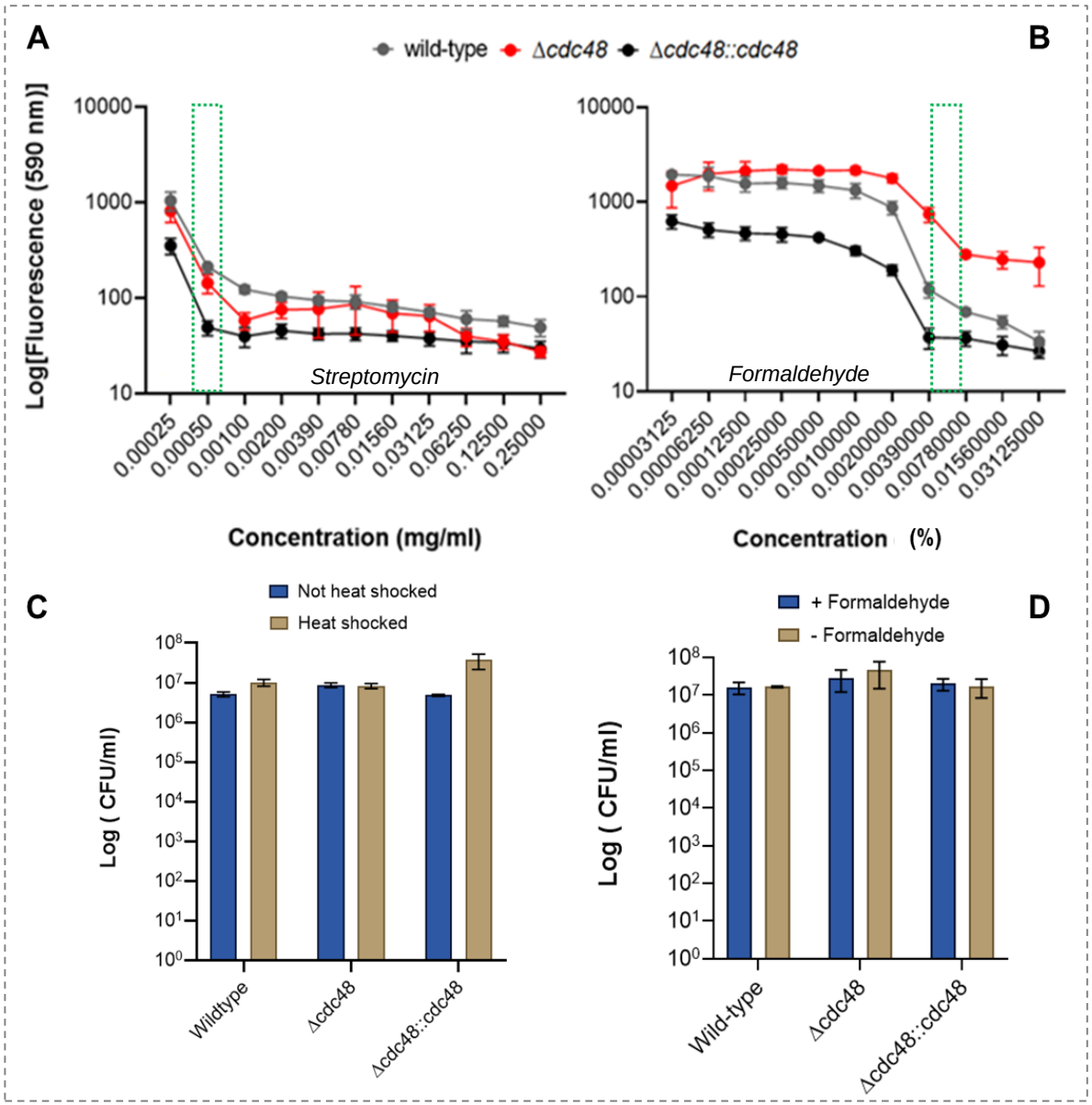

Figure 4.11. Determination of MICs for antibiotics targeting protein homeostasis or heat stress. Strains were grown to mid-exponential phase and then diluted appropriately. A starting concentration of 1 mg/ml for streptomycin (**A)** and 0.25% formaldehyde (**B**). Compounds were serially diluted across a 96-well plate. Each strain was added to each well (except for first row which served as a control) and incubated overnight (≥16 hours) at 37 °C. Following incubation, 10 µl of Alamar blue was added and further incubated at 37 °C for 3 – 5 hours. The reduction of resazurin was quantitated in a plate reader (excitation of 530-560nm and emission of 590nm). One plate was used per strain which included media and diluent controls. Data are representative of six independent repeats and error bars reflect the standard error from the mean (SEM). **Green boxes** represent approximate MIC_{50}. (**C**) Exponential phase cultures were exposed to heat stress (42 °C for 30 min). 'No heat' controls were also included. After treatment, CFU/ml were determined to establish viability. (**D**) Using the MIC_{50} previously determined, exponential phase cultures were equally divided - one contained a sub-minimum MIC_{50} (*0.005%*) of formaldehyde (i.e. 0.0015%) while the other served as an untreated control. After an overnight incubation at 37 °C, CFU\ml was determined to establish survival. For (C and D), data are representative three independent biological repeats. See supplementary figure C10 and C11 for MICs plates used to determine MICs values for streptomycin and formaldehyde.

There was non-significant antibiotic sensitivity for streptomycin and formaldehyde as the fold MICs was less than 2, respectively this was observed clearly in MICs plates. For heat sensitivity and formaldehyde exposure for CFUs there was no significance difference as the log difference was less 2, respectively. However log difference of 1.5 was observed for formaldehyde exposure suggesting cdc48 mutant was partial resistant to formaldehyde compared to wild-type.

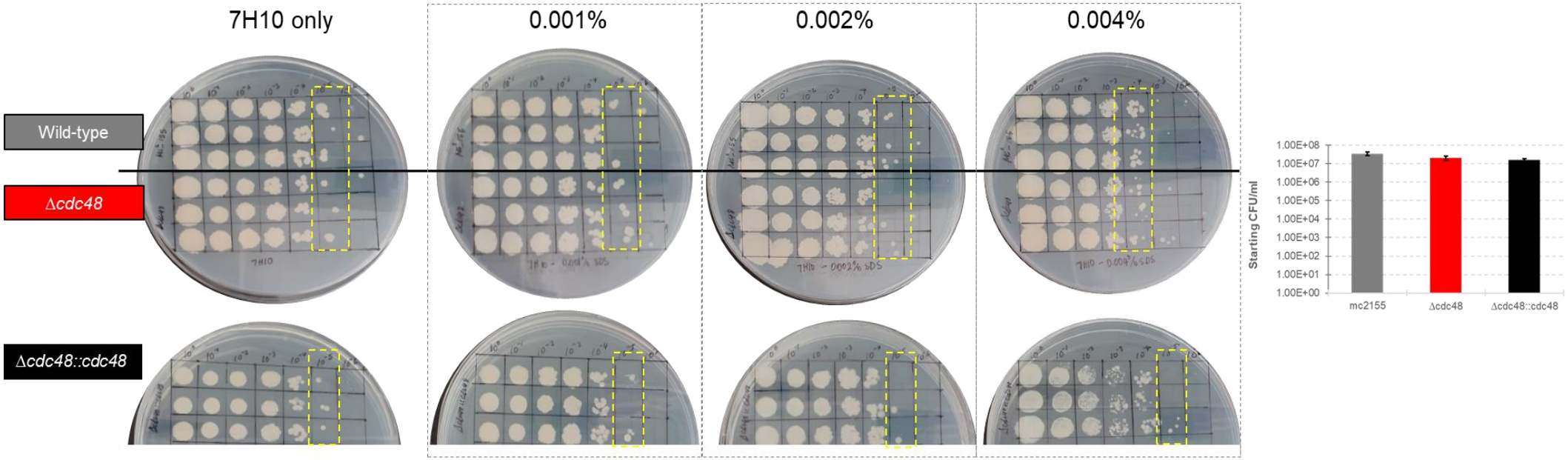

Figure 4.12. Survival following exposure to SDS was not adversely affected in *Msm* lacking Cdc48. Strains were grown to an OD_{600nm} of 0.5 and then serially diluted (from left to right, grids correspond to the 10^{0} – 10^{-6} dilutions). Ten microlitres of each dilution was plated on 7H10 media supplemented with the different concentration of SDS indicated. Plates were completely dried before incubating at 37 °C for 3 – 5 days. Emergent colonies were then manually scored to determine the level of SDS killing. **Yellow** boxes indicate the highest level of growth observed. Spotting experiments were performed in triplicate for each strain per one plate. Graphical insert on the right shows that the starting concentration of each strains (CFU/ml) was approximately equal. SDS killing for all strains was non-significant as killing started at 10^{-5} dilution for all concentration .

Heat-stress (42°C) was used to test the ability of each strain to. remove damaged proteins and to maintain overall stability of the proteome. As seen for formaldehyde exposure, heat-stress did not have a greater effect in the absence of Cdc48 as all strains displayed similar CFU/ml (10^6 - 10^7) relative to each other and the untreated controls (Figure 4.10C).

Finally, exposure to SDS (a protein-denaturing agent) was also tested to interrogate maintenance of the proteome. Like heat-stress and exposure to formaldehyde, the Δ*cdc48* strain was able to grow in the presence of up to 0.004% SDS which was comparable to the wild-type and Δ*cdc48::cdc48* (Figure 4.11). To be certain that no cell-density related effects were present, cultures used for spotting onto SDS were shown to be at roughly equal CFU/ml (~10^7) (Figure 4.11, insert). Taken together, all these data suggest that Cdc48 does not play a primary role in maintaining protein damage or turnover in *Msm*.

5. Discussion

Mycobacterium tuberculosis (Mtb), the causative agent of tuberculosis (TB), remains a global health burden (Raviglione and Sulis, 2016). Despite being treatable with antibiotics, the emergence of multi drug-resistant (MDR) and extensively drug-resistant (XDR) forms of *Mtb* has posed a significant challenge to TB therapy. This has necessitated the need to identify novel biological targets or anti-mycobacterial compounds. The mycobacterial cell wall is essential for cell survival and has been a TB drugs target for decades (Bhat et al., 2017). Targeting of AAA+ proteases has recently emerged as an interesting, novel approach (Alhuwaider and Dougan, 2017). AAA+ proteases, or the AAA+ protein family, and are found in all taxa. Thus, a drug with pharmacological activity specific to mycobacterial species will need to be developed to avoid to inhibition of the mammalian or human homologues.

This family of proteases is associated with various biological functions within a cell including transcription, recombination, DNA replication, remodelling of macromolecules complexes, protein quality, proteolysis, protein and nucleic translocation, cell division (Baek et al., 2013) and membrane fusion (Ogura and Wilkinson, 2001).

In this context, MSMEG_0858 (Cell Division Cycle 48 or Cdc48-like protein [Cpa]) has been identified as a potential drug target for development of anti-TB drugs but its physiological role remains poorly understood in mycobacteria (Alhuwaider and Dougan, 2017). A recent study suggested that the Cpa may play a broad role in *Msm* and other mycobacteria (Alhuwaider and Dougan, 2017). Under carbon starvation conditions, a *Msm* strain lacking Cpa showed growth defects and the levels of several hundred proteins were altered (greater than 3 fold) (Müller and Weber-Ban, 2019, Ziemski et al., 2018). Interestingly, Cdc48 (Cpa) was shown to interact with the low molecular weight penicillin binding protein, DacB (encoded by MSMEG_6113 or *dacB*), in *Msm* (Mashilo, 2018). DacB is a DD-carboxypeptidase (DD-CPase) associated with PG hydrolysis and is essential for viability. Furthermore, a study from the same group showed that depletion of DacB resulted in an alteration of PG biosynthesis, i.e. instead of the canonical, bi-polar mode of growth for mycobacteria, an increase in mono-polar growth was observed at a higher frequency (Ealand et al., 2019). Therefore, the interaction between Cdc48 (required for protein homeostasis) and DacB (a PG-associated enzyme) required further analysis.

In this study, the wild-type, a mutant strain lacking *cdc48* (*Δcdc48*) and its complemented derivative (*Δcdc48*::*cdc48*) were phenotypically characterized. As the mutant strains were previously constructed, the genotypes had to be independently confirmed. Three independent molecular techniques were used for this purpose – PCR, Southern hybridization and mRNA transcript analysis. By using primers flanking *cdc48*, the PCR showed that a mutant allele was present in Δ*cdc48*. In the complemented strain (Δ*cdc48::cdc48*), both the wild-type and mutant alleles were detected in addition to site-specific integration (at the *attB* site in the chromosome).

For thoroughness, a Southern hybridization confirmed the genomic context around the *cdc48* allele and in the Δ*cdc48::cdc48*. As expected, an mRNA transcript analysis showed that cdc48 was only detectable in the wild-type and Δ*cdc48::cdc48* strains. Taken together, all these results suggested that the strains used in this study were correct and could be further characterized.

Msm lacking *cdc48* was then grown in nutrient-rich (7H9) or nutrient-limited (carbon starvation) liquid media. In nutrient-rich conditions, the lack of *cdc48* had no effect on growth rate as cell density (OD_{600nm}) and viability (CFU/ml) remained unchanged relative to the wild-type strain. This suggested that *cdc48* could be required under more specific conditions. This was confirmed by a recent study that showed deletion of *cdc48* was associated with a decrease in growth rate when grown in carbon-starved media ((Ziemski et al., 2018)). This study replicated the experimental conditions used (i.e. carbon starvation) and confirmed the slow growth rate phenotype. This was consistent across cell density (lower OD_{600nm}) and viability (CFU/ml) after 24 hours of growth. Following complementation with the full-length *cdc48*, growth-rate was restored to wild-type levels suggesting that *cdc48* was specifically involved. Ziemsky *et al* (2018) also reported that the levels of hundreds of proteins were altered in Δ*cpa* in response to carbon starvation. DacB was not one of these proteins but the earlier interaction data (Mashilo *et al*., 2018) prompted us to assess the expression levels of *dacB* in the Δ*cdc48* background in response to carbon starvation. The rationale behind the method here was to see if the dacB expression will be affected or not in the absence of cdc48 under carbon starvation since growth defect was observed. In the wild-type strain, *dacB* levels were moderately greater than *cdc48*, but this pattern was not significantly altered when *cdc48* was absent.

The next step would have been to assess protein levels for each but we did not have access to purified, recombinant proteins or mono-clonal antibodies. Time constraints in the course of this MSc project did not allow for pursuit of this approach. Due to the slower growth rate of Δcdc48 in response to carbon starvation (at 24 hours) and the interaction with DacB, strains were stained

with the PG-specific probe, BADA. PG-specific probes can be used to determine sites of new PG synthesis or remodelling. In the wild-type strain, the predominant staining pattern was 'bipolar' which is consistent with the establish growth model for mycobacteria (i.e. growth via extension from both poles) y of cells with 'septa only'. This suggests that the Cdc48 protein is involve(Hannebelle et al., 2020, Botella et al., 2017, Kieser and Rubin, 2014, Meniche et al., 2014). A smaller proportion showed mono-polar staining and even less cells were associated with 'septal only', 'polar & septal', 'uniform staining across entire cell' and 'multi-septa'. In contrast, Δ*cdc48* was associated with altered PG staining patterns. For example, very few cells displayed 'bipolar' or 'mono-polar' staining but there was a significant increase in the frequency of cells with 'septa only' suggesting that *cdc48* may mediate some aspect of cell division which is yet to be explored. In addition, the frequency of cells with 'multiple septa' was almost double in Δcdc48. Since these phenotypes were not reversed in the complementation strain, we cannot assign this physiological role with certainty. Despite these altered PG staining patterns, cell length was not significantly different in all three strains tested which therefore necessitates that the PG staining patterns be explored further.

Various phenotypic tests were then conducted to elucidate the putative role of Cdc48 in cell division. The Δ*cdc48* strain was significantly more permeable to ethidium bromide uptake which suggested physical alterations in the cell wall and/or membrane. This led us to test whether compounds/conditions specifically targeting the cell wall or protein homeostasis was altered in the absence of *cdc48*. Amoxicillin is a β-lactam antibiotic which prevents the trans-peptidation reactions catalysed by high molecular weight penicillin binding proteins thereby limiting cross-link formation. This process leads to cell lysis (Akhavan and Vijhani, 2019).

D-cycloserine inhibits alanine racemase – an enzyme involved in the biosynthesis of uridine diphosphate (UDP)-*N*-acetylmuramyl-pentapeptide which is a precursor for cell wall PG (Lambert and Neuhaus, 1972). Lysozyme is a hydrolase that degrades the β-1-4 glycosidic bond

in the sugar backbone of PG causing cell lysis (Lesnierowski and Kijowski, 2007). Vancomycin prevents the synthesis of PG by binding tightly to peptides containing D-alanyl-D-alanine at the free carboxyl end (Watanakunakorn, 1984). Ultimately, compounds targeting the PG component of the cell wall (i.e. amoxicillin, vancomycin, lysozyme and D-cycloserine) were not more potent in Δ*cdc48*.

Similarly, compounds specifically targeting proteins showed no enhanced effects in Δ*cdc48* either since MIC_{50} values remained unchanged (i.e. streptomycin prevents protein synthesis by acting on ribosomes leading to misreading of the genetic code, inhibition of translation initiation of mRNA, and aberrant proofreading (Honoré and Cole, 1994) while formaldehyde irreversibly cross-links and inactivates proteins (Metz et al., 2004). Furthermore, exposure to heat-stress (42 °C for 30 min), sub-MIC_{50} of formaldehyde and SDS did not affect cells lacking *cdc48*.

6. Conclusion

Understanding the physiological role of Cdc48 in mycobacterial physiology may help us gain knowledge that is useful in elucidating the mechanisms of protein complexes that are essential for cell growth. This study confirmed that Cd48 is dispensable under nutrient-rich conditions. In contrasts, its function became more pronounced under carbon limited conditions suggestive of a specialist role. We further showed that Cdc48 is not required for cell viability under various stresses targeting i) the peptidoglycan in the cell wall, and ii) protein stability, synthesis and turnover.

7. Limitations of this study

The interaction of Cdc48 and DacB was not confirmed in this study. Using a molecular technique (other than the M-PFC assay as per Mashilo, 2018) such as co-immunoprecipitation was one of the aims and would have independently proven the interaction. Complementation of

the Δ*cdc48* strain was only partial – mRNA transcript analysis suggested that *cdc48* levels in Δ*cdc48::cdc48* were approximately 5 times lower than wild-type levels. Despite the carbon starvation growth phenotype being reversed following complementation with the full-length gene, the PG-staining phenotypes were not (particularly the 'septa only' and 'multi-septa' phenotypes suggesting altered cell-division). As a result, ascribing a cell division phenotype to Cdc48 can only be made cautiously and requires further investigation. Future work could interrogate the role of Cdc48 in other nutrient limiting conditions such as nitrogen or fatty acid starvation as these are directly applicable to the growth conditions faced by *M. tuberculosis in vivo*.

8. References

ABRAHAMS, K. A. & BESRA, G. S. 2016. Mycobacterial cell wall biosynthesis.

AGYEMAN, A. A. & OFORI-ASENSO, R. 2017. Tuberculosis—an overview. *Journal of Public Health and Emergency,* 1**,** 1-11.

AKHAVAN, B. J. & VIJHANI, P. 2019. Amoxicillin. *StatPearls [Internet]*.

ALDRIDGE, B. B., FERNANDEZ-SUAREZ, M., HELLER, D., AMBRAVANESWARAN, V., IRIMIA, D., TONER, M. & FORTUNE, S. M. 2012. Asymmetry and aging of mycobacterial cells lead to variable growth and antibiotic susceptibility. *Science,* 335**,** 100-104.

ALHUWAIDER, A. A. H. & DOUGAN, D. A. 2017. AAA+ machines of protein destruction in mycobacteria. *Frontiers in molecular biosciences,* 4**,** 49.

ANDREWS, J. R., NOUBARY, F., WALENSKY, R. P., CERDA, R., LOSINA, E. & HORSBURGH, C. R. 2012. Risk of progression to active tuberculosis following reinfection with Mycobacterium tuberculosis. *Clinical infectious diseases,* 54**,** 784-791.

ARICHA, S., KINGWARA, L., MWIRIGI, N., CHABA, L., KIPTAI, T., WAHOGO, J., OTWABE, J., ONYANGO, P., KARANJA, M. & AYIEKO, C. 2019. Comparison of GeneXpert and line probe assay for detection of Mycobacterium tuberculosis and rifampicin-mono resistance at the National Tuberculosis Reference Laboratory, Kenya. *BMC infectious diseases,* 19**,** 1-8.

BAEK, G. H., CHENG, H., CHOE, V., BAO, X., SHAO, J., LUO, S. & RAO, H. 2013. Cdc48: a swiss army knife of cell biology. *Journal of amino acids,* 2013.

BANSAL-MUTALIK, R. & NIKAIDO, H. 2014. Mycobacterial outer membrane is a lipid bilayer and the inner membrane is unusually rich in diacyl phosphatidylinositol dimannosides. *Proceedings of the National Academy of Sciences,* 111**,** 4958-4963.

BARANOWSKI, C., WELSH, M. A., SHAM, L.-T., ESKANDARIAN, H. A., LIM, H. C., KIESER, K. J., WAGNER, J. C., MCKINNEY, J. D., FANTNER, G. E. & IOERGER, T. R. 2018. Maturing *Mycobacterium smegmatis* peptidoglycan requires non-canonical crosslinks to maintain shape. *Elife,* 7**,** e37516.

BARRY, C. E., BOSHOFF, H. I., DARTOIS, V., DICK, T., EHRT, S., FLYNN, J., SCHNAPPINGER, D., WILKINSON, R. J. & YOUNG, D. 2009. The spectrum of latent tuberculosis: rethinking the biology and intervention strategies. *Nature Reviews Microbiology,* 7**,** 845-855.

BARTHELME, D. & SAUER, R. T. 2012. Identification of the Cdc48• 20S proteasome as an ancient AAA+ proteolytic machine. *Science,* 337**,** 843-846.

BESRA, G. & BRENNAN, P. 1997. The mycobacterial cell wall: biosynthesis of arabinogalactan and lipoarabinomannan. *Biochemical Society Transactions,* 25**,** 845-850.

BHAT, Z. S., RATHER, M. A., MAQBOOL, M., LAH, H. U., YOUSUF, S. K. & AHMAD, Z. 2017. Cell wall: a versatile fountain of drug targets in *Mycobacterium tuberculosis*. *Biomedicine & Pharmacotherapy,* 95**,** 1520-1534.

BOLSCHER, N., HOPPENBROUWERS, K. & BURGMEIJER, R. 2007. Tuberculose.

BOSHOFF, H. I. & BARRY, C. E. 2005. Tuberculosis—metabolism and respiration in the absence of growth. *Nature Reviews Microbiology,* 3**,** 70-80.

BOTELLA, H., YANG, G., OUERFELLI, O., EHRT, S., NATHAN, C. F. & VAUBOURGEIX, J. 2017. Distinct spatiotemporal dynamics of peptidoglycan synthesis between *Mycobacterium smegmatis* and *Mycobacterium tuberculosis*. *MBio,* 8.

BROWN, P. J., KYSELA, D. T. & BRUN, Y. V. Polarity and the diversity of growth mechanisms in bacteria. Seminars in cell & developmental biology, 2011. Elsevier, 790-798.

BUCHBERGER, A. 2013. Roles of Cdc48 in regulated protein degradation in yeast. *Regulated proteolysis in microorganisms***,** 195-222.

CHENGALROYEN, M. D., BEUKES, G. M., GORDHAN, B. G., STREICHER, E. M., CHURCHYARD, G., HAFNER, R., WARREN, R., OTWOMBE, K., MARTINSON, N. & KANA, B. D. 2016. Detection and quantification of differentially culturable tubercle bacteria in sputum from patients with tuberculosis. *American journal of respiratory and critical care medicine,* 194**,** 1532-1540.

COKER, R. J. 2004. Multidrug-resistant tuberculosis: public health challenges. *Tropical Medicine and International Health,* 9**,** 25-40.

DE MARTINO, M., LODI, L., GALLI, L. & CHIAPPINI, E. 2019. Immune response to *Mycobacterium tuberculosis*: a narrative review. *Frontiers in pediatrics,* 7**,** 350.

EALAND, CS, ASMAL, R, MASHIGO, L, CAMPBELL, L, KANA, BD. 2019. Characterization of putative DD-carboxypeptidase-encoding genes in *Mycobacterium smegmatis*. *Scientific Reports,* 9(1):5194.

FALZON, D., SCHÜNEMANN, H. J., HARAUSZ, E., GONZÁLEZ-ANGULO, L., LIENHARDT, C., JARAMILLO, E. & WEYER, K. 2017. World Health Organization

treatment guidelines for drug-resistant tuberculosis, 2016 update. *European Respiratory Journal,* 49.

FÖRSTER, F., SCHULLER, J. M., UNVERDORBEN, P. & AUFDERHEIDE, A. 2014. Emerging mechanistic insights into AAA complexes regulating proteasomal degradation. *Biomolecules,* 4**,** 774-794.

GANDHI, N. R., NUNN, P., DHEDA, K., SCHAAF, H. S., ZIGNOL, M., VAN SOOLINGEN, D., JENSEN, P. & BAYONA, J. 2010. Multidrug-resistant and extensively drug-resistant tuberculosis: a threat to global control of tuberculosis. *The Lancet,* 375**,** 1830-1843.

HAINES, D. S. 2010. p97-containing complexes in proliferation control and cancer: emerging culprits or guilt by association? *Genes & cancer,* 1**,** 753-763.

HANNEBELLE, M. T., VEN, J. X., TONIOLO, C., ESKANDARIAN, H. A., VUARIDEL-THURRE, G., MCKINNEY, J. D. & FANTNER, G. E. 2020. A biphasic growth model for cell pole elongation in mycobacteria. *Nature communications,* 11**,** 1-10.

HANSCHEID, T., RIBEIRO, C. M., SHAPIRO, H. M. & PERLMUTTER, N. G. 2007. Fluorescence microscopy for tuberculosis diagnosis. *Lancet. Infectious diseases (print),* 7**,** 236-237.

HARDING, C. V. & BOOM, W. H. 2010. Regulation of antigen presentation by *Mycobacterium tuberculosis*: a role for Toll-like receptors. *Nature Reviews Microbiology,* 8**,** 296-307.

HETT, E. C. & RUBIN, E. J. 2008. Bacterial growth and cell division: a mycobacterial perspective. *Microbiol. Mol. Biol. Rev.,* 72**,** 126-156.

HOAGLAND, D. T., LIU, J., LEE, R. B. & LEE, R. E. 2016. New agents for the treatment of drug-resistant *Mycobacterium tuberculosis*. *Advanced drug delivery reviews,* 102**,** 55-72.

HONORÉ, N. & COLE, S. T. 1994. Streptomycin resistance in mycobacteria. *Antimicrobial agents and chemotherapy,* 38**,** 238-242.

ISEMAN, M. D. 1993. Treatment of multidrug-resistant tuberculosis. *New England Journal of Medicine,* 329**,** 784-791.

JOYCE, G., WILLIAMS, K. J., ROBB, M., NOENS, E., TIZZANO, B., SHAHREZAEI, V. & ROBERTSON, B. D. 2012. Cell division site placement and asymmetric growth in mycobacteria. *PLoS One,* 7**,** e44582.

KIESER, K. J. & RUBIN, E. J. 2014. How sisters grow apart: mycobacterial growth and division. *Nature Reviews Microbiology,* 12**,** 550-562.

KREBS, S., FISCHALECK, M. & BLUM, H. 2009. A simple and loss-free method to remove TRIzol contaminations from minute RNA samples. *Analytical biochemistry,* 387**,** 136-138.

LAMBERT, M. P. & NEUHAUS, F. C. 1972. Mechanism of D-cycloserine action: alanine racemase from *Escherichia coli* W. *Journal of bacteriology,* 110**,** 978-987.

LESNIEROWSKI, G. & KIJOWSKI, J. 2007. Lysozyme. *Bioactive egg compounds.* Springer.

LOKHANDE, T. N. & PAWAR, M. S. D. 2019. TUBERCULOSIS: PATHOGENESIS, EMERGING DRUG TARGETS, CURRENT DRUG REGIMENS AND DRUGS IN CLINICAL DEVELOPMENT.

LÖNNROTH, K., CASTRO, K. G., CHAKAYA, J. M., CHAUHAN, L. S., FLOYD, K., GLAZIOU, P. & RAVIGLIONE, M. C. 2010. Tuberculosis control and elimination 2010–50: cure, care, and social development. *The Lancet,* 375**,** 1814-1829.

MACNEIL, A., GLAZIOU, P., SISMANIDIS, C., MALONEY, S. & FLOYD, K. 2019. Global epidemiology of tuberculosis and progress toward achieving global targets—2017. *Morbidity and Mortality Weekly Report,* 68**,** 263.

MAHOMED, H., HAWKRIDGE, T., VERVER, S., ABRAHAMS, D., GEITER, L., HATHERILL, M., EHRLICH, R., HANEKOM, W. A. & HUSSEY, G. D. 2011. The

tuberculin skin test versus QuantiFERON TB Gold® in predicting tuberculosis disease in an adolescent cohort study in South Africa. *PloS one,* 6**,** e17984.

MARAKALALA, M. J., RAJU, R. M., SHARMA, K., ZHANG, Y. J., EUGENIN, E. A., PRIDEAUX, B., DAUDELIN, I. B., CHEN, P.-Y., BOOTY, M. G. & KIM, J. H. 2016. Inflammatory signaling in human tuberculosis granulomas is spatially organized. *Nature medicine,* 22**,** 531-538.

MASHILO, P. 2018. *Characterization of Mycobacterial peptidoglycan remodelling enzymes.*

MELZER, E. S., SEIN, C. E., CHAMBERS, J. J. & SIEGRIST, M. S. 2018. DivIVA concentrates mycobacterial cell envelope assembly for initiation and stabilization of polar growth. *Cytoskeleton,* 75**,** 498-507.

MENICHE, X., OTTEN, R., SIEGRIST, M. S., BAER, C. E., MURPHY, K. C., BERTOZZI, C. R. & SASSETTI, C. M. 2014. Subpolar addition of new cell wall is directed by DivIVA in mycobacteria. *Proceedings of the National Academy of Sciences,* 111**,** E3243-E3251.

METZ, B., KERSTEN, G. F., HOOGERHOUT, P., BRUGGHE, H. F., TIMMERMANS, H. A., DE JONG, A., MEIRING, H., TEN HOVE, J., HENNINK, W. E. & CROMMELIN, D. J. 2004. Identification of formaldehyde-induced modifications in proteins: reactions with model peptides. *Journal of Biological Chemistry,* 279**,** 6235-6243.

MEYER, H. & WEIHL, C. C. 2014. The VCP/p97 system at a glance: connecting cellular function to disease pathogenesis. *Journal of cell science,* 127**,** 3877-3883.

MÜLLER, A. U. & WEBER-BAN, E. 2019. The bacterial proteasome at the core of diverse degradation pathways. *Frontiers in molecular biosciences,* 6**,** 23.

NARDELL, E. A. 2016. Transmission and institutional infection control of tuberculosis. *Cold Spring Harbor perspectives in medicine,* 6**,** a018192.

NEUWALD, A. F., ARAVIND, L., SPOUGE, J. L. & KOONIN, E. V. 1999. AAA+: A class of chaperone-like ATPases associated with the assembly, operation, and disassembly of protein complexes. *Genome research,* 9**,** 27-43.

NOSS, E. H., HARDING, C. V. & BOOM, W. H. 2000. *Mycobacterium tuberculosis* inhibits MHC class II antigen processing in murine bone marrow macrophages. *Cellular immunology,* 201**,** 63-74.

OGURA, T. & WILKINSON, A. J. 2001. AAA+ superfamily ATPases: common structure–diverse function. *Genes to Cells,* 6**,** 575-597.

RAMAKRISHNAN, L. 2012. Revisiting the role of the granuloma in tuberculosis. *Nature Reviews Immunology,* 12**,** 352-366.

RAVIGLIONE, M. & SULIS, G. 2016. Tuberculosis 2015: burden, challenges and strategy for control and elimination. *Infectious disease reports,* 8**,** 33-37.

SCHEFFERS, D.-J. & PINHO, M. G. 2005. Bacterial cell wall synthesis: new insights from localization studies. *Microbiology and molecular biology reviews,* 69**,** 585-607.

SIBINELLI-SOUSA, S., HESPANHOL, J. T. & BAYER-SANTOS, E. 2021. Targeting the Achilles' Heel of Bacteria: Different Mechanisms To Break Down the Peptidoglycan Cell Wall during Bacterial Warfare. *Journal of Bacteriology*, 203.

SINGH, B., NITHARWAL, R. G., RAMESH, M., PETTERSSON, B. F., KIRSEBOM, L. A. & DASGUPTA, S. 2013. Asymmetric growth and division in M ycobacterium spp.: compensatory mechanisms for non-medial septa. *Molecular microbiology,* 88**,** 64-76.

SINGH, R., DWIVEDI, S. P., GAHARWAR, U. S., MEENA, R., RAJAMANI, P. & PRASAD, T. 2020. Recent updates on drug resistance in *Mycobacterium tuberculosis*. *Journal of applied microbiology,* 128**,** 1547-1567.

SQUEGLIA, F., RUGGIERO, A. & BERISIO, R. 2018. Chemistry of Peptidoglycan in Mycobacterium tuberculosis Life Cycle: An off-the-wall Balance of Synthesis and Degradation. *Chemistry–A European Journal,* 24**,** 2533-2546.

Suleiman, K. 2017. Tuberculosis Diagnostic Tools. Available from https://www.treatmentactiongroup.org/wp-content/uploads/2017/04/TB-Diagnostics-Guide.pdf. Accessed on the 2021 June 11.

TORRECILLA, I., OEHLER, J. & RAMADAN, K. 2017. The role of ubiquitin-dependent segregase p97 (VCP or Cdc48) in chromatin dynamics after DNA double strand breaks. *Philosophical Transactions of the Royal Society B: Biological Sciences,* 372**,** 20160282.

UNCIULEAC, M.-C., SMITH, P. C. & SHUMAN, S. 2016. Crystal structure and biochemical characterization of a *Mycobacterium smegmatis* AAA-Type nucleoside triphosphatase phosphohydrolase (Msm0858). *Journal of bacteriology,* 198**,** 1521-1533.

WATANAKUNAKORN, C. 1984. Mode of action and in-vitro activity of vancomycin. *Journal of Antimicrobial Chemotherapy,* 14**,** 7-18.

World Health Organizaion (WHO) 2013. Global tuberculosis report 2013.

World Health Organization (WHO). www. who. int/tb/publications/global_report/high_tb_burdencountrylists2016-2020. pdf? ua= 1.

World Health Organization (WHO) 2017. Guidelines for treatment of drug-susceptible tuberculosis and patient care.

WU, Y., HU, K., LI, D., BAI, L., YANG, S., JASTRAB, J. B., XIAO, S., HU, Y., ZHANG, S. & DARWIN, K. H. 2017. Mycobacterium tuberculosis proteasomal ATPase Mpa has a β-grasp domain that hinders docking with the proteasome core protease. *Molecular microbiology,* 105**,** 227-241.

ZIEMSKI, M., JOMAA, A., MAYER, D., RUTZ, S., GIESE, C., VEPRINTSEV, D. & WEBER-BAN, E. 2018. Cdc48-like protein of actinobacteria (Cpa) is a novel proteasome interactor in mycobacteria and related organisms. *Elife*, 7**,** e34055.

Supplementary Information

Appendix A: Media and solutions

Table A1: Media and supplements.

Media / supplements	Components
Middlebrook 7H9	4.7 g Difco Middlebrook 7H9 powder and 2ml glycerol dissolved in 986 ml sdH_2O. Autoclave (sterilisation temperature - 121°C, sterilisation time - 25 min and exhaust percentage - 0%). Once media has to cooled sufficiently (~60°C), add 10 ml 100X glucose salts and 2 ml Tween80 (25%)
Middlebrook 7H10	19 g Difco Middlebrook 7H10 powder and 5ml glycerol dissolved in 985 ml sdH_2O. Autoclave (sterilisation temperature - 121°C, sterilisation time - 15 min and exhaust percentage - 0%). Once media has to cooled sufficiently (~60°C), add 10 ml 100 X glucose salts.
Tween 80 (25%)	10 ml Tween80 dissolved in 40 ml sdH2O

Table A2: Solutions used for *Msm* DNA extractions.

Solutions	Components

TE buffer	10 mM Tris- HCl (pH 8) and 10 mM EDTA dissolved in sdH_2O. Autoclave (sterilisation temperature - 121°C, sterilisation time -25 min and exhaust percentage - 0%).
CTAB/NaCl	4.1% NaCl and 10% N – acetyl- N, N, N – trimethyl ammonium bromide dissolved in sdH_2O. Filter sterilize using a 0.2 µm pore size.

Table A3: Solutions used for DNA precipitation

Solutions	Components
Chloroform:Isoamyl alcohol	24 ml chloroform and 1ml isoamyl alcohol
Sodium Acetate	3 M sodium acetate dissolved in sdH2O (pH5.2). Autoclave

Table A4. Solutions used for DNA electrophoresis

Solutions	Components
1X TAE	50 X stock solution: 242 g Tris base 57.1 ml glacial acetic and 100 ml EDTA (pH 8) made up to 1L with sdH2O.
Ethidium Bromide	10 mg/ml dissolved in sdH_2O.

Table A5. Agarose gel recipes

Gel percentage	**Amount of agarose (g) in 50 ml TAE**
1	0.5

Table A6: Solutions for Southern hybridizations

Solutions	**Components**

Denaturation solution	1.5 M NaCl and 0.5 M NaOH dissolved in sdH2O.
Depurination solution	0.25 M HCl dissolved in sdH2O.
TBE (1X**)**	100 ml 10 X Tris-Borate-EDTA (Sigma) dissolved in 900 ml sdH2O.
SSC (20X)	0.3 M Sodium citrate and 3 M NaCl dissolved in sdH2O.
SDS (10%)	10 g SDS powder dissolved in 100 ml sdH2O.
Solution 1	0.1% SDS and 2 X SSC dissolved in sdH2O
Solution 2	0.1% SDS and 0.5 X SSC dissolved in sdH2O.
Maleic Acid Buffer	1.5 M NaCl and 1 M Maleic acid dissolved in sdH2O. Adjusted to pH 7.5 with NaOH pellets
Wash buffer	0.1 M Maleic Acid Buffer and 0.3% Tween20
Blocking solution (Roche)	1 X blocking solutions dissolved in Maleic Acid Butter.
Detection buffer	0.1 M NaCl and 0.1 M Tris-HCl dissolved in sdH2O (pH 9.5)
Antibody solution (Roche)	Dilute 1: 10000 in blocking solution.
CSPD (Roche)	Disodium 3-(4-methoxysoiro {1, 2-dioxetane-3, 2‟-(5‟-chloro) tricycle [3.3.1.13,7] decan}-4-yl)phenyl phosphate
Stripping solution	0.2 M NaOH and 0.1% SDS dissolved in sdH2O.

Appendix B: Primers

Table B1: Primers used for confirmation of *Msm* strains using PCR.

Primer name	DNA sequence	Expected size of amplicon
Cdc48_KO_conf_F	5'–CAG CCA TCC GGA GTC GTG GGA–3'	mc^2 _155= 2527 bp
MSMEG_0858_KO_conf_R1	5'-CAGATCGAGGTCCTCGGACGG-3'	Δ*cdc48* = 493 bp
MSMEG_0858_KO_conf_R2	5'–CTG TGG CGC TGG GAA CTG–3'	Δ*cdc48::cdc48* = 493 bp

Table B2: Primers used for confirmation of *Msm* strains using southern blot.

Primers	DNA sequence	Expected size of amplicon

MSMEG_0858 US _F MSMEG_0858 US _R MSMEG_0858 DS_F MSMEG_0858 DS_R	5'–GTC CAG CAT TCC CCC GAT G–3' 5'–GCA GCG CGG AGG TGT TCA G–3' 5'–GTC ACG GCC GCC GAC GTC–3' 5'–TGG GCA GAA CCG TGT TGG–3'	1500 bp expected for the upstream (US) and downstream (DS) regions.

Table B3: Primers used for confirmation of site specific integration of complementing vector.

Primer name	DNA sequence	Expected size of amplicon
ATTB_BS1 ATTP_L2	5'– ACG TGG CGG TCC CTA CCG–3' 5'–CTT GGA TCC CGC TGC GC–3'	382bp
ATTB_BS2 ATTP_L4	5'–ACA GGA TTT GAA CCT GCG GC–3' 5'–AAT TCT TGC AGA CCC TGG A–3'	320bp

Table B4: Primers used for confirmation of gene expression using qPCR.

Primer name	DNA sequence	Expected size of amplicon
Set 1 MSMEG_0858_F MSMEG_0858_R	 5'–ACCCGCCGCGCGGCGTGC –3' 5'–GAGCCGACCCATTTGTCC–3'	None
Set 2 MSMEG_0858_F	5'–ACCTATCGACCCGGCCGT–3' 5'–TGTCGAGGTCGACATCAT–3'	None

Appendix C: Supplementary Figures

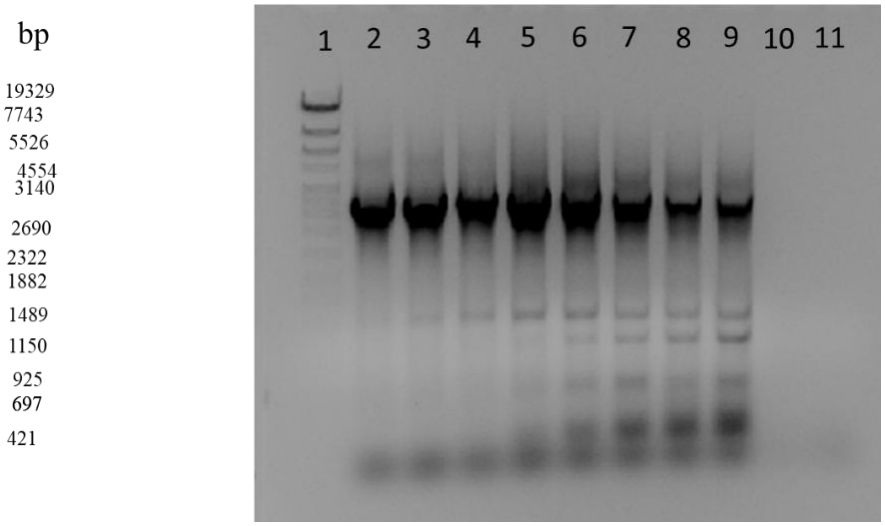

Figure C1. Gradient PCR using wild-type DNA as template to amplify MSMEG_0858 gene. Lane 1 **(**Marker III), lane (2-9) mc^2155 sample 1-9, lane (10) empty, lane (11) no DNA control. From lane 2 to 9 annealing temperatures were as follows 65, 64, 63, 61.3, 58.8, 56.9, 55.7, 55, 50 °C and for NTC was 61.1 °C. The optimal temperature used for primers was 65 °C.

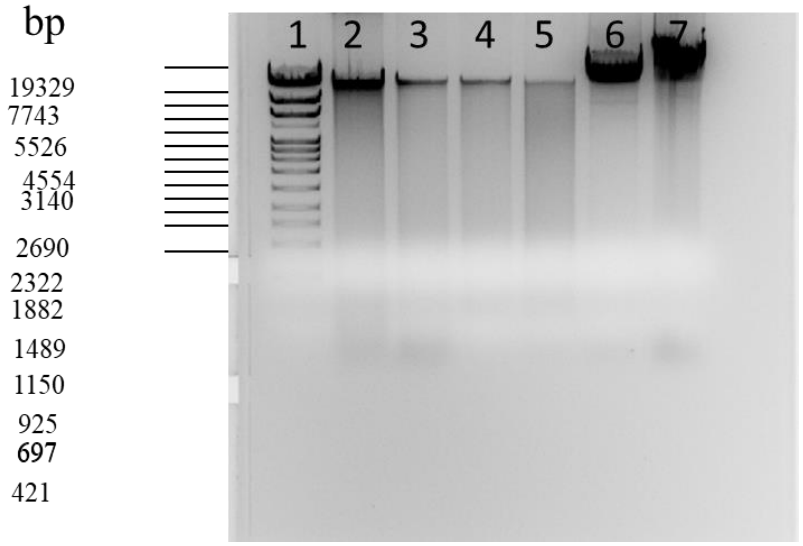

Figure C2. Optimization of genomic DNA extractions. Lane (1) marker VI, lane (2-3) wild-type, lane (4-5) Δ*cdc48* mutant strain, lane (6-7) Δ*cdc48::cdc48*, complementation strain.

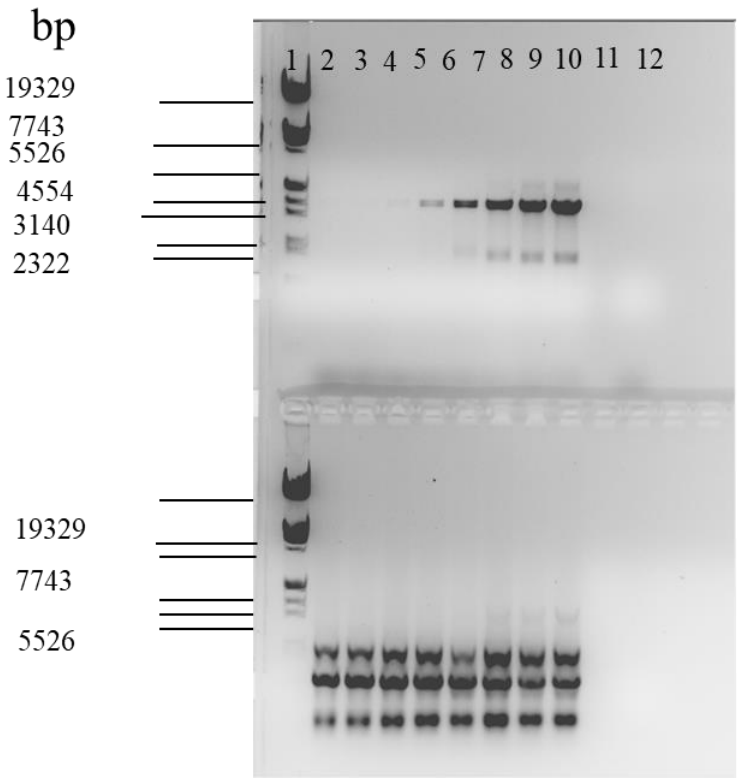

Figure C3. Gradient PCR of upstream and downstream region (1500bp) of *cdc48*. Top: upstream region, Lane (1) Marker VI, lane (2-9) sample 1-9. Bottom downstream region lane (1) marker VI, lane (2-9) sample 1-9, lane (10) no DNA control. Temperature gradient was set up as follows from lane 2 to 9, 68, 67.8, 67.4, 66.5, 66.2, 65.6, 65, 62.2, 60 and for NTC 63.7°C. The optimal temperature for upstream region primers was 66.5 °C and downstream region primers were non-specific as multiple bands were observed.

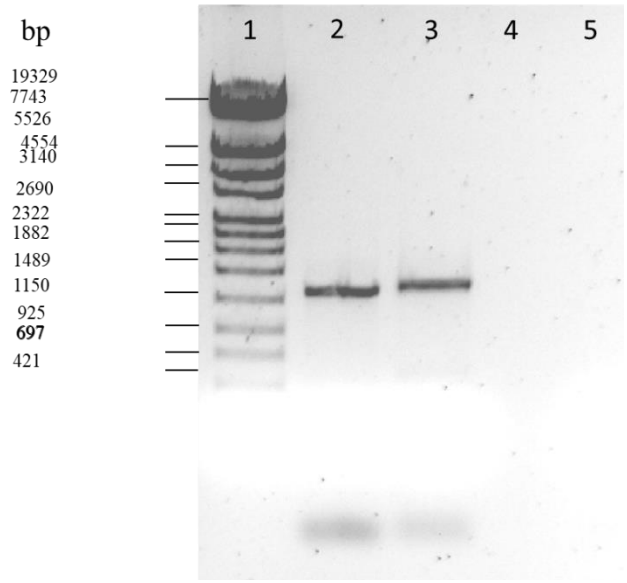

Figure C4. Probe specific to cdc48 allele designed with DIG kit. Lane (1) marker VI, lane (2) cold PCR, lane (3) hot PCR and lane (4) no DNA template.

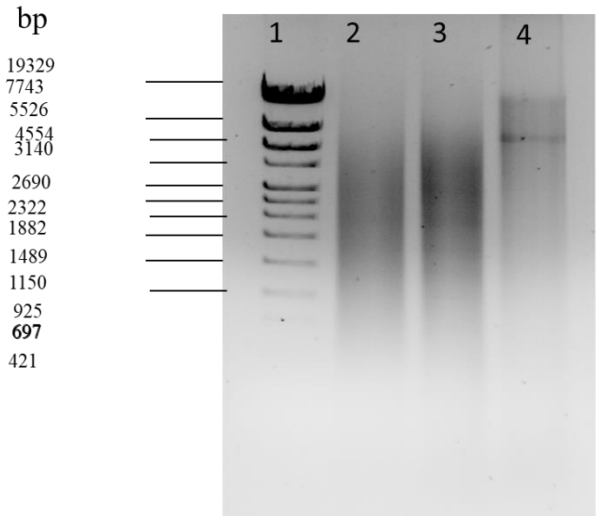

Figure C5. gDNA digestion for southern blot analysis. Lane (1) marker VI, lane (2) wild-type, lane (3) cdc48 mutant, lane (4) complemented mutant strain and lane (5) maker VI.

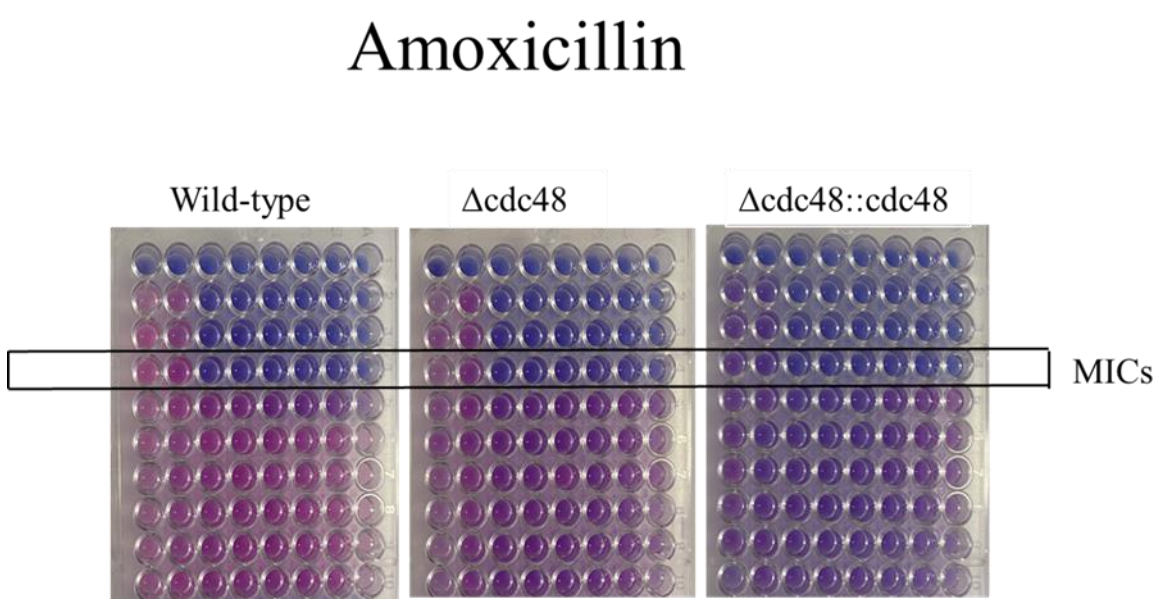

Figure C6. Amoxicillin MICs plate. Strains were grown to mid-exponential phase and the diluted appropriately. A starting concentration of 1 mg/ml was used following serially dilution across a 96-well, round-bottom plate. Each strain was added to each well (except for first row which served as a control) and incubated overnight (≥16 hours) at 37 °C without shaking. Following incubation, 10 µl of Alamar blue was added and further incubated at 37 °C for 3 – 5 hours. Conversion of resazurin (Alamar blue) occurs in response to cellular metabolic reduction and is accompanied by a change from blue to fluorescent pink (only viable cells can reduce the compound). Fluorescence was quantitated in a plate reader (excitation of 530-560nm and emission of 590nm). One plate was used per strain which included media and diluent controls. Data are representative of the mean for six independent repeats and error bars reflect the standard error from the mean. Black box represents MIC value of amoxicillin.

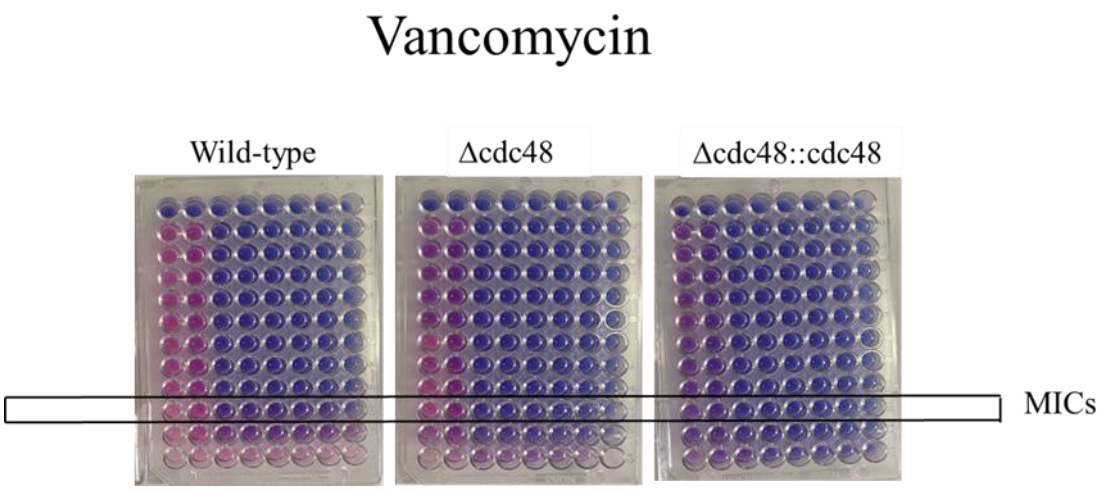

Figure C7. Vancomycin MICs plate. Strains were grown to mid-exponential phase and the diluted appropriately. A starting concentration of 1 mg/ml was used followed by serially dilution across a 96-well, round-bottom plate. Each strain was added to each well (except for first row which served as a control) and incubated overnight (≥16 hours) at 37 °C without shaking. Following incubation, 10 µl of Alamar blue was added and further incubated at 37 °C for 3 – 5 hours. Conversion of resazurin (Alamar blue) occurs in response to cellular metabolic reduction and is accompanied by a change from blue to fluorescent pink (only viable cells can reduce the compound). Fluorescence was quantitated in a plate reader (excitation of 530-560nm and emission of 590nm). One plate was used per strain which included media and diluent controls. Data are representative of the mean for six independent repeats and error bars reflect the standard error from the mean. Black box represents MIC value of vancomycin.

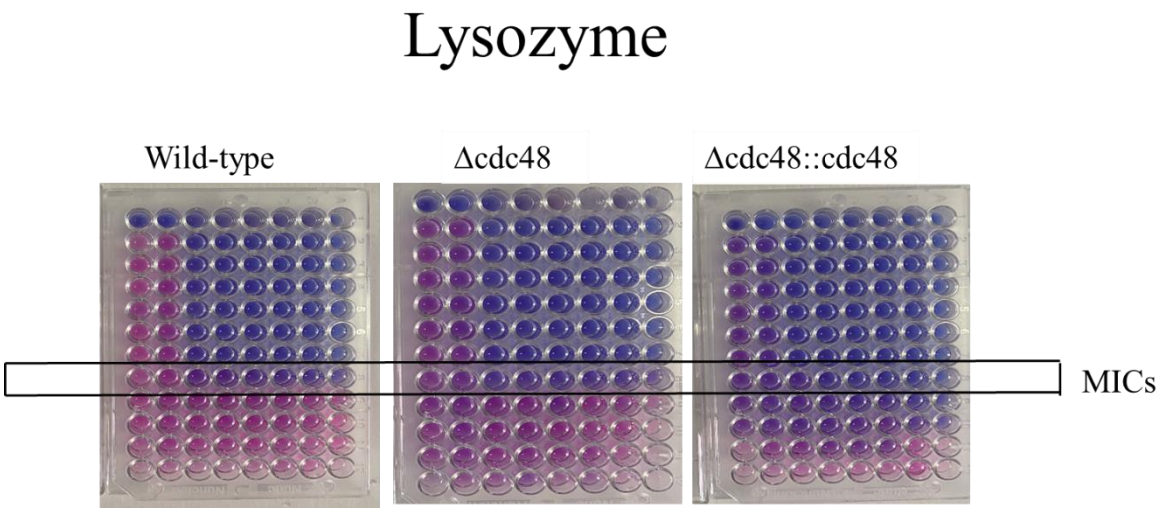

Figure C8. Lysozyme MICs plate. Strains were grown to mid-exponential phase and the diluted appropriately. A starting concentration of 50 µg/ml for lysozyme was used followed by serially diluted across a 96-well, round-bottom plate. Each strain was added to each well (except for first row which served as a control) and incubated overnight (≥16 hours) at 37 °C without shaking. Following incubation, 10 µl of Alamar blue was added and further incubated at 37 °C for 3 – 5 hours. Conversion of resazurin (Alamar blue) occurs in response to cellular metabolic reduction and is accompanied by a change from blue to fluorescent pink (only viable cells can reduce the compound). Fluorescence was quantitated in a plate reader (excitation of 530-560nm and emission of 590nm). One plate was used per strain which included media and diluent controls. Data are representative of the mean for six independent repeats and error bars reflect the standard error from the mean. Black box represents MIC value of lysozyme.

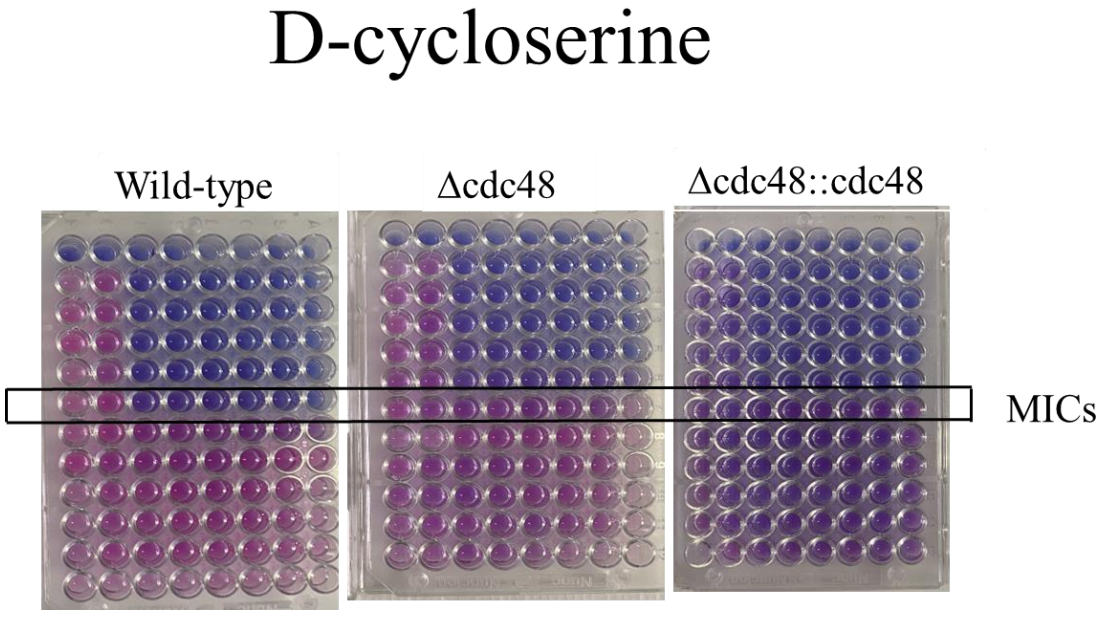

Figure C9. D-cycloserine MICs plate. Strains were grown to mid-exponential phase and the diluted appropriately. A starting concentration of 1 mg/ml was used followed by serially diluted across a 96-well, round-bottom plate. Each strain was added to each well (except for first row which served as a control) and incubated overnight (≥16 hours) at 37 °C without shaking. Following incubation, 10 µl of Alamar blue was added and further incubated at 37

°C for 3 – 5 hours. Conversion of resazurin (Alamar blue) occurs in response to cellular metabolic reduction and is accompanied by a change from blue to fluorescent pink (only viable cells can reduce the compound). Fluorescence was quantitated in a plate reader (excitation of 530-560nm and emission of 590nm). One plate was used per strain which included media and diluent controls. Data are representative of the mean for six independent repeats and error bars reflect the standard error from the mean. Black box represents MIC value of D-cycloserine.

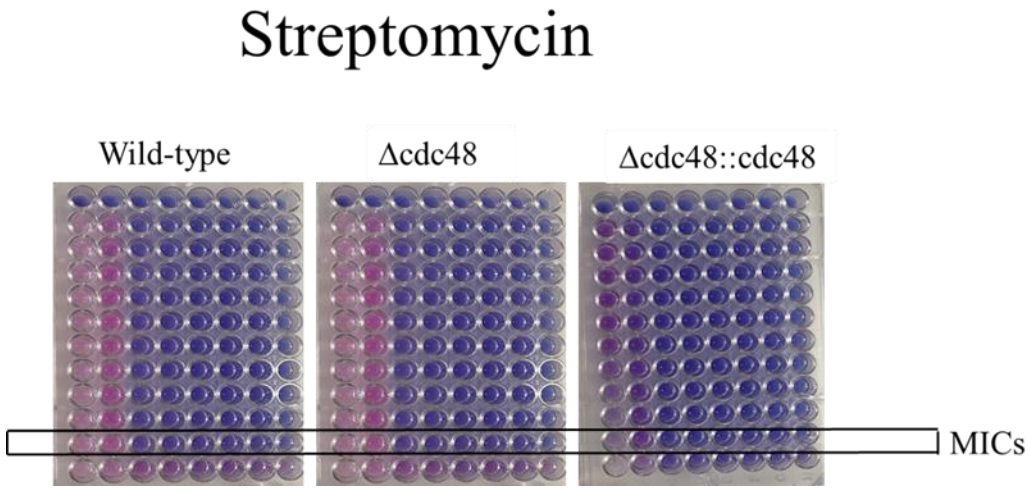

Figure C10. Streptomycin. MICs plate. Strains were grown to mid-exponential phase and the diluted appropriately. A starting concentration of 1 mg/ml was used followed by serially diluted across a 96-well, round-bottom plate. Each strain was added to each well (except for first row which served as a control) and incubated overnight (≥16 hours) at 37 °C without shaking. Following incubation, 10 µl of Alamar blue was added and further incubated at 37 °C for 3 – 5 hours. Conversion of resazurin (Alamar blue) occurs in response to cellular metabolic reduction and is accompanied by a change from blue to fluorescent pink (only viable cells can reduce the compound). Fluorescence was quantitated in a plate reader (excitation of 530-560nm and emission of 590nm). One plate was used per strain

which included media and diluent controls. Data are representative of the mean for six independent repeats and error bars reflect the standard error from the mean. Black box represents MIC value of streptomycin.

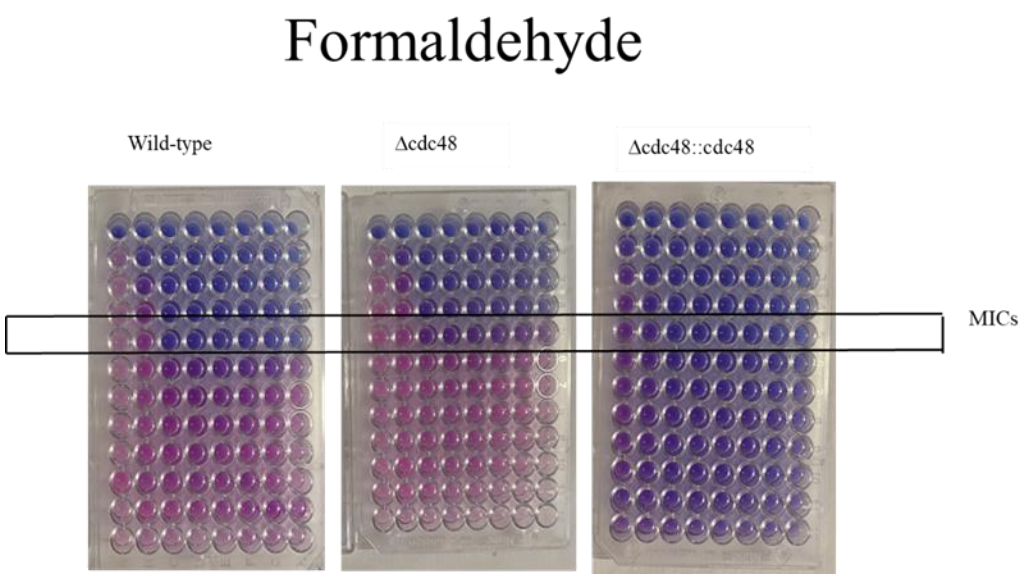

Figure C11. Formaldehyde MICs plate. Strains were grown to mid-exponential phase and the diluted appropriately. A starting concentration of 0.25 % was used followed by serially diluted across a 96-well, round-bottom plate. Each strain was added to each well (except for first row which served as a control) and incubated overnight (≥16 hours) at 37 °C without shaking. Following incubation, 10 µl of Alamar blue was added and further incubated at 37 °C for 3 – 5 hours. Conversion of resazurin (Alamar blue) occurs in response to cellular metabolic reduction and is accompanied by a change from blue to fluorescent pink (only viable cells can reduce the

compound). Fluorescence was quantitated in a plate reader (excitation of 530-560nm and emission of 590nm). One plate was used per strain which included media and diluent controls. Data are representative of the mean for six independent repeats and error bars reflect the standard error from the mean. Black box represents MIC value of formaldehyde.